Can we achieve atmospheric chemical environments in the laboratory? An integrated model-measurement approach to chamber SOA studies

Authors

Hannah S. Kenagy[1*], Colette L. Heald[1†], Nadia Tahsini[2], Matthew B. Goss[1], and Jesse H. Kroll[1,2]

Affiliations

[1]Department of Civil and Environmental Engineering, Massachusetts Institute of Technology, Cambridge, MA, USA.

[2]Department of Chemical Engineering, Massachusetts Institute of Technology, Cambridge, MA, USA.

[†]Now at: Institute for Atmospheric and Climate Science, ETH Zürich, Zürich, Switzerland

* Corresponding Author. Email: hskenagy@mit.edu

Abstract

Secondary organic aerosol (SOA), atmospheric particulate matter formed from low-volatility products of volatile organic compound (VOC) oxidation, impacts both air quality and climate. Current 3D models, however, cannot reproduce the observed variability in atmospheric organic aerosol. Because many SOA model descriptions are derived from environmental chamber experiments, our ability to represent atmospheric conditions in chambers directly impacts our ability to assess the air quality and climate impacts of SOA. Here, we develop a new approach that leverages global modeling and detailed mechanisms to design chamber experiments that mimic the atmospheric chemistry of organic peroxy radicals (RO_2), a key intermediate in VOC oxidation. Drawing on decades of laboratory experiments, we develop a framework for quantitatively describing RO_2 chemistry and show that no previous experimental approaches to studying SOA formation have accessed the relevant atmospheric RO_2 fate distribution. We show proof-of-concept experiments that demonstrate how SOA experiments can access a range of atmospheric chemical environments and propose several directions for future studies.

Introduction

Atmospheric aerosols are integral to two of today's most important environmental concerns: air pollution and climate. Exposure to aerosol pollution is associated with over 8 million premature deaths each year, making it the leading environmental risk factor for premature mortality (*1*, *2*). Atmospheric aerosols also impact the global climate by absorbing and scattering sunlight, as well as by altering cloud properties, with these impacts representing the largest source of uncertainty in our understanding of global radiative forcing (*3*). Organic aerosol (OA) constitutes a large, and sometimes dominant, fraction of fine aerosol mass (*4*). Much of this OA is secondary (secondary organic aerosol, SOA) (*4*, *5*), produced from volatile organic compounds (VOCs) that are oxidized in the atmosphere to form lower-volatility species. Despite the importance of SOA in the atmosphere and the decades of SOA-focused laboratory experiments, field measurements, and modeling studies, the complex chemical processing that leads to SOA formation is still not well constrained (*6*).

The first laboratory experiments examining SOA formation were recorded by Tyndall in the late 19th century; he observed the formation of a 'blue cloud' when irradiating organic vapors in a glass tube and attributed his observations to the formation of particles (*7*). Haagen-Smit's 'smog chamber' experiments in the 1950s demonstrated that a mixture of vehicular hydrocarbon pollutants (e.g., alkenes), O_3, and NO_2 formed particles upon irradiation by sunlight, helping to explain the

chemistry of urban smog (*8*). Later, Went (*9*) extended these experiments to include the oxidation of natural hydrocarbons, and postulated that photochemistry involving biogenic VOCs contributed 'blue hazes' in the atmosphere. 'Smog chamber' experiments throughout the 1980s continued to show evidence for SOA production from photochemistry involving biogenic and anthropogenic VOCs with O_3 and NO_x (*10*, *11*).

By 1990, researchers began to quantitatively determine SOA yields for oxidation of individual VOCs (*11*, *12*), which would eventually enable yield-based parameterizations in atmospheric models. A dependence of SOA yields on NO_x concentrations emerged from these chamber experiments, suggesting that atmospheric SOA formation depends on the chemical environment (*13–16*). Because of this observed NO_x-dependence, studies began to characterize experiments by their initial hydrocarbon-to-NO_x ratio as is common in descriptions of tropospheric ozone formation (*13*, *14*, *16*). The mechanism for the dependence of SOA yield on this ratio was initially uncertain, but by 1999 it was generally assumed to solely result from the changes in the relative importance of different oxidants (e.g. OH, O_3, NO_3) with varying NO_x concentrations (*17*, *18*). The first regional and global models of SOA also reflected this understanding: NO_x influences on O_3 and OH were included, but SOA yields for a given oxidant were assumed not to vary with NO_x concentration (*19–21*).

In the early- and mid-2000s, chamber studies demonstrated that changes in SOA yields with NO_x were a result of both changes in oxidant ratios and changes in the fate of RO_2, organic peroxy radicals produced in most VOC oxidation processes (*22*). For example, chamber experiments demonstrated that the relative importance of hydroperoxides (products of the reaction of RO_2 radicals with HO_2) to the oxidation product distribution could help explain the dependence of the SOA yield on NO_x (*23–25*). With the understanding that RO_2 chemistry is influenced by NO_x concentrations (*26*, *27*), chamber experiments were designed to access 'limiting conditions' in which the fate of RO_2 was dominated entirely by reaction with a single co-reactant: 'low-NO' experiments were designed to mimic 'clean' atmospheric conditions with RO_2+HO_2 as the dominant RO_2 fate, whereas 'high-NO' experiments were designed to mimic 'polluted' atmospheric conditions with RO_2+NO dominating RO_2 reactivity (*27–32*). The development of a chemical coordinate to track the competition between NO and HO_2 for reaction with RO_2 followed; this coordinate was gradually refined and by 2010 was defined by Pye et al. (*33*) as:

$$\beta = \frac{k_{RO_2+NO}[NO]}{k_{RO_2+NO}[NO]+k_{RO_2+HO_2}[HO_2]} \qquad \text{Equation (1)}$$

Using SOA yields measured under limiting RO_2 fate conditions, β could be interpreted as a 'mixing parameter' to estimate SOA yields at intermediate-NO_x conditions (*34*, *35*). By the late 2000s, SOA parameterizations in global models began to reflect the newly understood importance of NO_x for RO_2 fate by incorporating β-based SOA parameterizations (*33*, *36–38*).

Recent chamber experiments, however, have demonstrated that SOA yields may also depend on three additional RO_2 fates: RO_2 isomerization, RO_2+NO_2, and RO_2+RO_2 reactions (Figure 1). Laboratory and computational studies over the last decade have demonstrated that for some RO_2 species, unimolecular isomerization pathways have sufficiently short lifetimes (τ_{uni}) that they can be competitive with bimolecular reactions (i.e., $\tau_{uni} \leq \tau_{bi}$, where τ_{bi} is the RO_2 lifetime to bimolecular reactions) (*39*, *40*). Such isomerization reactions and subsequent rapid molecular oxygen additions can lead to the production of highly oxidized products, which can contribute to the formation of low-volatility SOA (*41*). Recent chamber studies have also demonstrated that the NO/NO_2 ratio during an experiment, which controls what fraction of acyl-RO_2 ($RC(=O)O_2$) react with NO versus NO_2, has a measurable effect on the oxidative product distribution and/or amount of SOA formed. At lower NO/NO_2 ratios, RO_2+NO_2 reactions can dominate the chemistry of acyl-

RO_2 radicals, thereby altering the oxidative product distribution and increasing the formation of peroxy acyl nitrates (PANs) (*42*, *43*) which can have an influence on SOA formation (*44*). Other chamber studies have demonstrated that SOA yields are affected by the RO_2/HO_2 ratio, which controls what fraction of RO_2 react with HO_2 versus with other RO_2 radicals (*23*, *45–47*). The direction and magnitude of this effect on SOA yields is determined by the volatility of RO_2+RO_2 products, which include alkoxy radicals (RO+RO), alcohol and carbonyl products (ROH+R'CHO), and organic peroxides (ROOR)). Numerous studies have highlighted ROOR products in particular as potential contributors to SOA formation (*48–50*). As such, current evidence indicates that four bimolecular RO_2 fates (reactions with NO, HO_2, NO_2, and RO_2), as well as unimolecular RO_2 reactions, may all affect SOA formation.

Current model parameterizations of SOA that include NO_x dependence, however, are still based on chamber experiments run under high-NO and low-NO extremes, with the untested assumption that SOA yields can be parameterized as a linear combination of yields measured at the two limiting cases (β=0 and β=1). By design, these 'limiting condition' experiments include high radical abundances that shorten the RO_2 bimolecular lifetime, thereby limiting RO_2 isomerization, and do not control for the role of RO_2+NO_2 or RO_2+RO_2 reactions. Moreover, experiments run at limiting 'high-NO' and 'low-NO' conditions that underlie today's model parameterizations are likely not fully relevant for SOA produced over multiple generations in the atmosphere, since the RO_2 fate might differ from one generation of oxidation to the next. As a result, current model parameterizations of SOA are mimicking SOA produced under idealized chamber conditions rather than representing realistic atmospheric chemical environments. This likely contributes to the inability of current large-scale models to reproduce the observed variability in atmospheric OA (*51*, *52*).

Because model parameterizations are informed by laboratory experiments, model accuracy hinges on the atmospheric relevance of both the physical and chemical conditions of laboratory experiments. Porter et al. (*53*) identified that chamber studies of SOA are often run under dry, room-temperature conditions, which are not representative of much of the atmosphere, and began to quantify what chemical space chamber experiments of SOA need to match in order to represent the atmosphere. Further quantification of atmospheric and chamber chemical environments and development of strategies for maximizing overlap between the two is the focus of this work.

Given the importance of bimolecular and unimolecular RO_2 chemistry for SOA production, here we define a four-parameter chemical space that allows us to track the fate of RO_2 in both the atmosphere and in laboratory studies. We use these parameters in conjunction with global modeling to define the chemical environments in which SOA is formed in the atmosphere, and we use mechanistic box modeling of environmental chambers to assess what parts of this chemical space are accessible in the laboratory. We discuss the challenges associated with mimicking the atmospheric chemical environment in chamber studies, show proof-of-concept experiments that demonstrate how SOA experiments can access a range of atmospheric chemical environments, and present pathways forward for furthering our understanding of SOA production in the atmosphere in light of the challenges.

Results

Atmospheric RO_2 fate distribution

A complete, quantitative description of RO_2 fates is needed to fully characterize an atmospheric chemical environment (*54*). Though β describes the competition between RO_2+HO_2 and RO_2+NO reactions, the contributions of RO_2 isomerization, RO_2+RO_2 reactions, and RO_2+NO_2 reactions to

atmospheric RO_2 reactivity necessitate additional chemical coordinates to fully describe the RO_2 fate distribution. Here we combine four parameters (β, τ_{bi}, RO_2/HO_2, and NO/NO_2) which have been used independently to characterize subsets of RO_2 reaction pathways (*23*, *33*, *44*, *53*, *55*, *56*) to complete a parameter space that fully describes atmospheric RO_2 fates as outlined in Figure 1. To our knowledge, this is the first time that these parameters have been considered together, and that more than one has been considered at a time, to describe RO_2 chemistry in the atmosphere and within chambers.

We adopt the bimolecular RO_2 lifetime against reaction with NO and HO_2, as originally defined by Teng et al. (2017):

$$\tau_{bi} = \frac{1}{k_{RO_2+NO}[NO]+k_{RO_2+HO_2}[HO_2]} \quad \text{Equation (2)}$$

A comparison between τ_{bi} and τ_{uni}, the RO_2 lifetime to unimolecular isomerization, indicates the relative contribution of bimolecular and unimolecular reactions. We also adopt the RO_2/HO_2 ratio to quantify the relative importance of RO_2+RO_2 chemistry and thus ROOR formation (*23*), as well as the NO/NO_2 ratio to denote the relative importance of PANs to the RO_2 fate (*43*, *44*). Ideally a ratio of rates (analogous to β) instead of a ratio of radical concentrations (RO_2/HO_2 and NO/NO_2) would be used to define the relative importance of RO_2+RO_2 and RO_2+NO_2 reactions to the RO_2 fate distribution, and a complete τ_{bi} definition would also include the lifetime of RO_2 against reaction with other RO_2 and with NO_2. However, because RO_2+RO_2 rate constants are both highly variable and uncertain (*48*, *49*), here we use the RO_2/HO_2 ratio to indicate the relative importance of RO_2+RO_2 reactions and omit RO_2+RO_2 reactions from the τ_{bi} determination (Eq. 2). Similarly, because RO_2+NO_2 reactions only produce stable products for acyl-RO_2, we use the NO/NO_2 ratio instead of a ratio of rates to simplify accounting and omit RO_2+NO_2 reactions from the τ_{bi} calculation, noting that τ_{bi} will be shorter for acyl-RO_2 than for other RO_2 (Eq. 2) .

To examine the fate of RO_2 in the atmosphere, we focus our analysis here on the oxidation of isoprene. Multi-generation isoprene oxidation is an important contributor to global SOA production (*36*), and the gas-phase oxidation chemistry of isoprene (including its RO_2 chemistry) has been studied extensively over the last decade (*57*). We also include a parallel set of analyses for monoterpene-derived SOA (Figures S1-S2); the results for monoterpenes are similar to those presented here for isoprene.

Understanding atmospheric RO_2 chemistry requires identifying which parts of the 4D chemical space defined here are populated during VOC oxidation in the atmosphere. Figure 2 shows the atmospheric distribution of β, τ_{bi}, RO_2/HO_2, and NO/NO_2 for isoprene-derived RO_2, calculated from hourly output from the GEOS-Chem chemical transport model (version 13.4.0, https://doi.org/10.5281/zenodo.7254268) for January and July 2016. We show the entire calculated global distribution of these four parameters, weighted by the rate of isoprene+OH oxidation; as such, any references to the 'atmospheric distribution' refer to the atmospheric distribution in regions where isoprene is undergoing OH-initiated oxidation (and any references to isoprene oxidation refer to OH-initiated oxidation), unless otherwise specified.

We note that the use of a global chemical transport model means our analysis is inherently at coarse spatial resolution (here 2°x2.5°), a scale relevant for considering global SOA production where most isoprene oxidation occurs. However, the model does not capture the distribution of RO_2 fates at fine spatial scales. For example, highly polluted environments would likely tend toward higher β and lower τ_{bi} than seen in the global distribution, resulting in conditions where RO_2+NO reactions are more likely to dominate the RO_2 reactivity. Even so, as NO_x emissions decrease in cities as a

result of emissions controls, values of τ_{bi} in urban areas are increasing (*58*), meaning future urban chemical environments may be better reflected in the global distributions shown here.

As shown in Figure 2, β spans the full possible range but, in most regions of the global atmosphere, does not lie at either extreme (median = 0.44, 25th percentile = 0.27, 75th percentile = 0.61). Rather, the 'intermediate-β' values that dominate the distribution indicate that RO_2 bimolecular reactions with NO and HO_2 are in competition with each other throughout most of the global atmosphere.

Moreover, values of τ_{bi} mostly lie between 20 and 300 seconds throughout the atmosphere (Figure 2a). Within this distribution, τ_{bi} is generally longer in regions with lower β (where reaction with HO_2 dominates) and shorter in higher-β environments (where reaction with NO dominates). The relative importance of RO_2 isomerization is determined by the relative rates of each process (i.e., τ_{bi} vs. τ_{uni}). However, values of τ_{uni} are highly variable, as RO_2 isomerization rates are highly structure-dependent and vary over orders of magnitude for different RO_2. In some cases, isomerization is fast ($\tau_{uni} \ll 1$ s), meaning it will dominate throughout virtually the entire atmosphere (*55*, *59*). In contrast, the atmospheric fate of any RO_2 with very slow isomerization rates ($\tau_{uni} > 1{,}000$ s) will be dominated by bimolecular reactions. RO_2 radicals with intermediate τ_{uni} that are within an order of magnitude of atmospheric τ_{bi} (i.e., 1 s < τ_{uni} < 1,000 s), per contra, may react by both bimolecular and unimolecular pathways in the atmosphere. Additionally, we note that the temperature dependence of unimolecular isomerization rates is much steeper than the temperature dependence of most bimolecular RO_2 reactions (*39*, *55*); as such, the relative importance of unimolecular and bimolecular reactions for a given RO_2 in the atmosphere can change with temperature. However, the temperature variability for regions of the atmosphere with substantial isoprene oxidation is relatively narrow (10th percentile = 285 K, median = 295 K, 90th percentile = 302 K).

Figure 2b also shows that atmospheric RO_2/HO_2 ratios are largely below 1 and generally increase as β decreases. Determining the relative importance of RO_2+HO_2 and RO_2+RO_2 reactions relies critically on uncertain and variable RO_2+RO_2 rate constants. Assuming an RO_2+RO_2 rate constant of 10^{-12} at 298 K (*49*), an average atmospheric RO_2/HO_2 ratio of ~0.5 indicates that 5% of RO_2+peroxy radical reactions in the atmosphere are RO_2+RO_2. Faster RO_2+RO_2 rate constants of 10^{-11} and 10^{-10} (*48*) would suggest that 33% and 83%, respectively, of RO_2+peroxy radical reactions are RO_2+RO_2.

The atmospheric NO/NO_2 ratio is centered around 0.4 (Figure 2c) and is largely controlled by O_3 abundance and NO_2 photolysis rates. In the GEOS-Chem mechanism, this average value corresponds to net formation (production minus loss) of PANs in ~90% of atmospheric acyl-RO_2+NO_x reactions at atmospheric temperatures.

RO_2 fate distributions during SOA chamber experiments: previous experiments and challenges

The global distributions of RO_2 fates in the atmosphere shown in Figure 2 can be viewed as providing 'targets' for RO_2 chemistry in laboratory studies. However, as shown in Figure 3, previous SOA chamber experiments have generally simulated RO_2 reactivities that differ substantially from those in the atmosphere. The classic smog photochemistry chamber experiments of the 1990s (e.g., Griffin et al., 1999), involving the irradiation of hydrocarbon-NO_x mixtures, achieved the high-β conditions typical of highly polluted urban areas, but at much lower values of τ_{bi} and NO/NO_2 than are typical in the atmosphere. The 'limiting condition' SOA experiments of the mid-2000s (e.g., Kroll et al., 2005, 2006; Ng et al., 2007a) achieved the extreme-β conditions they were designed for, but they did not capture all possible atmospheric RO_2 isomerization

products, nor did they fully match atmospheric distributions of RO_2/HO_2 and NO/NO_2 ratios (*60*, *61*). Traditional dark ozonolysis experiments (*62*) did access atmospheric τ_{bi}, but achieved RO_2/HO_2 ratios much higher than those found in the atmosphere. Recent ultraclean experiments measuring HOM yields from ozonolysis at low NO concentrations in the CLOUD chamber (*63*) accessed a range of β at longer RO_2 lifetimes, but also had RO_2/HO_2 ratios that far exceeded than those of the atmosphere. Oxidation flow reactors (OFRs), which can be considered as a limiting case for small chambers, have become increasingly popular for studying SOA formation over longer aging timescales. Though OFRs can access the full range of β (*64*, *65*), most OFR experiments have accessed τ_{bi} for RO_2 that are shorter than those in the atmosphere (*66*, *67*). Further details about the chemical environments achieved in these previous approaches are included in Section S1.

Though the aforementioned previous approaches to SOA studies span a wide range of RO_2 fates, no previous approach has overlapped with the atmospheric distribution of RO_2 reactivity. The longstanding challenges in matching atmospheric conditions in SOA chamber experiments derive from two fundamental laboratory constraints (Figure 4): (1) a sufficiently high quantity of products is needed to surpass instrumental limits of detection (LOD), and (2) oxidation timescales must be fast enough to outcompete lab-specific loss processes, namely wall loss and dilution. In order to produce enough OA to surpass instrument LODs (~1 μg m^{-3}), experiments must start with large quantities of the VOC precursor (typically 100s of ppbC). Together, the need for large precursor concentrations and the requirement for fast oxidation timescales mean that experiments must be run at relatively high oxidant levels, resulting in the production of high HO_2 and RO_2 concentrations and/or requiring the addition of large amounts of NO. Ultimately, the chemical conditions of the chamber are driven by the VOC oxidation itself, in contrast to the atmosphere where the ambient chemical environment controls VOC oxidation conditions. When VOC oxidation controls the chemical environment, which is the case not only in standard laboratory experiments but also in outdoor perturbation experiments where a VOC is added to a chamber filled with ambient air, control of RO_2 reaction conditions can be challenging.

Possible RO_2 fates in chamber experiments of SOA formation

A key question is what chemical conditions can be accessed in laboratory chamber experiments measuring SOA yields and to what extent chambers can span the range of RO_2 reaction conditions found in the global atmosphere (as shown in Figure 2). Using a box model with near-explicit chemistry (F0AM (*68*) with MCM v3.3.1 (*69*, *70*)), we assess the RO_2 fate distribution accessible during photochemical isoprene oxidation in a typical environmental chamber at 298 K, as shown in Figure 5. We span combinations of initial concentrations of H_2O_2, HONO, and NO with 100 ppb initial isoprene, a mixing ratio sufficiently high to allow for SOA yield measurements. For each simulated experiment, we determine whether the initial conditions allow for two generations of oxidation during an 8-hour experiment, and for those experiments that satisfy this criterion, we assess the corresponding distribution of RO_2 fates. The results we present here use experimental parameters (dilution rates, light intensities) from a single chamber (the 7.5 m^3 MIT environmental chamber (*71*)), but the overall conclusions are applicable to most indoor environmental chambers. The challenges presented here would be exacerbated in smaller-volume chambers (including OFRs) because the timescales for dilution and wall loss are shorter, necessitating even higher oxidant concentrations.

Figure 5 shows results from these box-modeling simulations. The entire range of β between 0 and 1 can be achieved by careful selection of precursor concentrations. Achieving atmospheric RO_2/HO_2 ratios is possible at intermediate and high β, but is more difficult at low β, when very

high quantities of H_2O_2 are required to achieve sufficiently fast oxidation (*72*). However, RO_2 speciation also differs between chambers and the atmosphere: CH_3O_2 is ≈ 50% of atmospheric RO_2 whereas it only makes up ≈1-10% of chamber RO_2 (Figure S3). As such, chamber RO_2+RO_2 product distributions likely differ from those in the atmosphere. NO/NO_2 ratios are generally lower in chamber conditions than in the atmosphere as a result of high HO_2 concentrations (see Figure S4) and low NO_2 photolysis rates (j_{NO2}). While increasing the chamber light intensity would result in increased NO/NO_2 ratios, the high chamber HO_2 concentrations preclude reaching atmospheric NO/NO_2 ratios even at atmospheric j_{NO2}.

With various initial conditions, bimolecular lifetimes (τ_{bi}) between 2 and 20 seconds can be achieved at low β, but are orders of magnitude lower at high β. At moderate β, experimental conditions can access τ_{bi} in the 10s of seconds, but the lower oxidant levels at these longer τ_{bi} mean it becomes increasingly difficult to achieve two generations of oxidation in an 8-hour experiment. However, in order to capture the atmospheric distribution of bimolecular and unimolecular RO_2 products in a chamber experiment, it is not always necessary to have values of τ_{bi} in the chamber directly overlap with those in the atmosphere. Instead, experiments need only to access a regime where the relative importance of bimolecular and unimolecular reactions is largely the same as it is in the atmosphere. Accessing atmospherically relevant RO_2 fates for RO_2 with fast or slow isomerization ($\tau_{uni} < 1$ s or $\tau_{uni} > 1{,}000$ s) is achievable with many combinations of initial conditions in the chamber. Careful selection of initial conditions is required, however, for RO_2 with intermediate isomerization rates (1 s < τ_{uni} < 1,000 s) to ensure that competition between bimolecular and unimolecular fates in the chamber match that of the atmosphere.

In the case of isoprene, eight different first-generation RO_2 radicals are formed, but only two (the Z-δ isomers) undergo isomerization reactions at atmospheric conditions. Both Z-δ isomers isomerize rapidly enough (4-OH Z-δ τ_{uni} = 0.3 s, 1-OH Z-δ τ_{uni} = 3 s at 297 K (*55*)) that isomerization almost always outcompetes their bimolecular reactions in the atmosphere. SOA chamber experiments can mimic atmospheric conditions where the fates of these RO_2 are dominated by isomerization across the entire β range for the 4-OH Z-δ isomer and at high- and intermediate-β for the 1-OH Z-δ isomer. Low-β experiments can achieve conditions in which isomerization outcompetes bimolecular reactions of the 1-OH Z-δ RO_2 but cannot access atmospheric conditions where isomerization entirely *dominates* the 1-OH Z-δ RO_2 fate. We note that β and τ_{bi} derived from GEOS-Chem shown in Figure 5 are calculated at the corresponding atmospheric temperatures and pressures, whereas the β and τ_{bi} that describe chamber chemistry are all calculated at 298 K. Over the range of atmospheric isoprene oxidation temperatures, however, variation in τ_{uni} for isoprene-derived RO_2 is constrained to within an order of magnitude (shaded rectangles in Figure 5) and therefore does not significantly alter the atmospheric competition between bimolecular and unimolecular fates for isoprene-derived RO_2.

Ratios of oxidants also vary between extreme-β experiments and intermediate-β experiments. As shown in Figure S5, extreme-β experiments can access conditions in which nearly all the isoprene is oxidized by OH, without contributions from other oxidants (O_3 and NO_3). At β=0, the lack of NO prevents production of O_3 or NO_3, while at β=1, there is sufficient excess of NO to titrate away any O_3 and NO_3 produced. However, at intermediate-β conditions, photochemical cycling will produce O_3 and NO_3, which will persist because the levels of NO are too low to titrate them. In fact, intermediate-β experiments involve OH/O_3 ratios that are similar to those in regions of the atmosphere characterized by intermediate-β conditions. NO_3 concentrations at intermediate-β, however, will be higher in most indoor chambers compared to daytime tropospheric conditions because of the lower visible light intensities. The presence of multiple oxidants does complicate experimental interpretation and subsequent model parameterization since most current model SOA

parameterizations are based on yields for a single oxidant. However, the SOA produced during intermediate-β experiments is arguably more representative of atmospheric photochemical SOA production than single-oxidant studies.

Changes in chemical conditions during an experiment resulting from the oxidation of both NO_x and VOCs are another consideration during intermediate-β experiments (*73*). The decreases in NO concentrations over time lead to reductions in β and increases in τ_{bi}. As shown in Figure S6, changes in τ_{bi} over a typical experiment are on the order of seconds to tens of seconds. Changes in β vary and are minimized at the extremes, but intermediate-β experiments can transverse nearly the full range of β values over time, and these time-dependent changes in chemical conditions make it more challenging to locate these experiments in chemical space. Addition of a small amount of NO (or NO precursor) throughout an experiment (*28*, *64*, *74*) may reduce the time-dependent changes in chemical conditions.

Chamber experiments spanning a range of RO_2 fates

Using the global model- and box model-informed approach to experimental design described here, we carried out a series of isoprene+OH oxidation chamber experiments. In Figure 6, we focus on three experiments that span the chamber-accessible β-τ_{bi} parameter space. These proof-of-concept experiments are, to our knowledge, the first that explicitly and systematically attempt to span the atmospheric chemical environment during SOA production, despite the aforementioned challenges. Initial conditions for these experiments (shown in Table S1) are used as box modeling inputs to predict RO_2 fate parameters (β and τ_{bi}) for each experiment. To assess whether we achieved the predicted ranges of β and τ_{bi} in these experiments, we examine the first-generation gas-phase oxidative product distribution, shown in Figure 6 and Figure S9. At low-β conditions (β=0.02), the first-generation product distribution is dominated, as expected, by $C_5H_{10}O_3$; this corresponds to ISOPOOH, the main product formed from RO_2+HO_2 chemistry. At intermediate- and high-β conditions (β=0.61 and 1.0, respectively), isoprene hydroxy nitrate ($C_5H_9O_4N$, the RO_2+NO termination product) becomes an increasingly larger contributor to the product distribution. The relative importance of the isomerization product (HPALD, $C_5H_8O_3$) to the product distribution is highest at intermediate-β conditions in which τ_{bi} is expected to be highest. These first-generation gas-phase product distribution trends confirm that our experiments did indeed span ranges of β and τ_{bi}, demonstrating that chamber experiments can be run under a wider range of atmospheric RO_2 fates than have been accessed previously.

The limitations of our experimental instrumentation preclude measurements of unique RO_2+RO_2 and RO_2+NO_2 products. However, modeling of our experiments indicates that the relative contribution of these pathways to RO_2 fate in our experiments is in line with what is shown in Figure 5: RO_2/HO_2 ratios fall within the atmospheric RO_2/HO_2 distribution whereas NO/NO_2 ratios are far below the atmospheric NO/NO_2 distribution. As a result of the high HO_x concentrations in typical chamber SOA experiments, faster photolysis rates or higher NO concentrations than those under typical atmospheric photochemical conditions are required to achieve atmospheric NO/NO_2 ratios.

Discussion

Pathways forward

The results of the proof-of-concept experiments described above confirm the possibility of designing and executing experiments to mimic many of the key features of the atmospheric chemical environment in laboratory chambers, including chemical environments where multiple

RO_2 fates compete (e.g., the intermediate-β, longer-τ_{bi} experiment in Figure 6). As such, this model-informed approach to experimental design represents a useful approach for future chamber experiments of SOA production. The next generation of SOA chamber studies and model treatments of SOA production, however, must find ways to tackle the remaining challenges. Here, we suggest some directions for future research aimed at enabling progress in our understanding of SOA formation chemistry.

As discussed earlier, one of the key limitations of SOA chamber experiments is the need to produce enough products such that they surpass instrument limits of detection. This is particularly challenging for VOCs with low SOA yields, such as isoprene. The ability to measure SOA mass concentrations with ng/m^3-level sensitivity would relax this constraint, allowing experiments to be run with lower initial VOC concentrations. For example, as shown in Figure S7, longer τ_{bi} are accessible during experiments with lower initial isoprene concentrations, including τ_{bi} up to 200 s for high-β experiments initialized with 0.1 ppb isoprene, because of lower HO_2 and RO_2 concentrations. Such improvements to analytical instrumentation for measuring OA mass, especially for experiments with added seed particles, could involve increased sensitivity for hard-ionization quantitative aerosol mass measurements (e.g., the aerosol mass spectrometer or aerosol chemical speciation monitor) as well as the development of sensitive (non-mass spectrometric) approaches for measuring OA mass. Better quantification methods for highly sensitive soft ionization techniques (e.g., chemical ionization mass spectrometry and extractive electrospray ionization mass spectrometry) could also help relax this constraint.

Quantifying SOA yields through new particle formation (NPF) could alleviate some of the LOD constraint by improving signal-to-noise ratios. However, ultrafine particles produced during nucleation events are lost to chamber walls more quickly than the accumulation mode particles typically present during seeded experiments. Therefore, NPF experiments that accommodate multi-generation chemistry require large chambers and fast oxidation, resulting in increased HO_x concentrations and thus altering the radical balance.

In addition, inclusion of the role of all RO_2 reactions involved in SOA formation may require more complex SOA parameterizations in models. The untested linear mixing assumption between RO_2+NO and RO_2+HO_2 yields should at least be tested, and SOA parameterizations may need to increase in complexity to account for more than two RO_2 fates. For example, existing RO_2-fate-based SOA parameterizations that include SOA yields for RO_2+HO_2 and RO_2+NO (*37*) may need to include yields for other RO_2 reaction pathways. Future experimental work is required, however, to evaluate how much a given RO_2 reaction pathway actually affects atmospheric SOA production and therefore how many dimensions are required to accurately model SOA formation chemistry. If SOA yields do not vary significantly over the atmospheric ranges of an RO_2 fate, that reaction pathway does not need to be carefully studied or included in models. For example, variation within the atmospheric distribution of τ_{bi} are likely to matter only for systems with isomerization reactions that have lifetimes within an order of magnitude of atmospheric τ_{bi} (i.e., 1 s < τ_{uni} < 1,000 s). Recent work has demonstrated that SOA yields from some monoterpene reactions are sensitive to RO_2/HO_2 only when this ratio is changed dramatically (*47*, *75*), suggesting that the atmospheric variation of RO_2/HO_2 between 0 and 2 has an insignificant effect on biogenic SOA yields. Other laboratory studies, however, have suggested that this narrow atmospheric range may affect SOA yields from anthropogenic VOCs (*46*). Additional experiments have shown that isoprene SOA yields more than halve between NO/NO_2 ≈ 0.1 and 0.3 (*44*), suggesting that changes in NO/NO_2 across the range found in the atmosphere (≈ 0.2-0.7) can affect isoprene SOA yields. Similar tests are required across these atmospheric ranges for an assortment of VOCs.

An alternative to the parameterized approach for modeling SOA production is a semi-mechanistic approach, which describes SOA formation in terms of key condensable species generated from gas-phase chemical mechanisms. This approach combines laboratory measurements of gas-phase products with estimates of their volatilities to predict particle-phase products and aerosol yields and was recently implemented in the Community Regional Atmospheric Chemistry Multiphase Mechanism (CRACMM) (*76*). Such an approach has the advantage of inherently including the effects of changes in atmospheric variables (e.g., RO_2 chemistry, temperature) on SOA production, in contrast to a parameterized approach where such effects require explicit consideration. However, a semi-mechanistic approach generally requires uncertain estimates of oxidation product volatilities as well as thoughtful consideration of what species are included given resource constraints, and predicted SOA formation has generally not been validated by yields measured in laboratory studies. More model species will also increase computational demand, and so may not be appropriate for large-scale models, including global chemistry-climate and/or Earth system models.

Regardless of the model approach used to describe SOA formation, a crucial component is continual interfacing between laboratory measurements, models, and field observations. Updated laboratory-based model predictions of SOA should be compared to ambient observations, and further experiments should then be targeted to chemical environments in which the model-measurement difference is greatest. Validation of model SOA descriptions against SOA yields measured in chamber experiments that match the atmospheric chemical environment will also aid model parameterization and further development.

Conclusions

The mechanistic advances in our understanding of RO_2 chemistry over the last two decades have enabled us to replace the high- and low-NO_x binary used in the past to describe RO_2 fates with a more nuanced description of the complex, multi-dimensional space that controls the product distribution of atmospheric VOC oxidation. Leveraging 3D- and box-modeling tools with our understanding of the complexity of RO_2 chemistry along with careful control of chamber inputs will help ensure that experimental resources are dedicated to experiments that span chemical parameter spaces that best match those of the atmosphere.

Because laboratory studies are the foundation for model parameterizations of SOA, their limitations inherently become the limitations of models. Modeling SOA based on experiments run at extreme-β conditions has major shortcomings: extreme-β conditions do not describe the chemical environment in most of the atmosphere, the assumption of linearity between extremes has never been tested, and extreme-β chamber conditions generally do not mimic the role of other RO_2 reactions (RO_2 isomerization, RO_2+RO_2, and RO_2+NO_2) that may occur in the atmosphere. However, improvements are possible, via the use of modeling to explicitly design the chemical environment for SOA chamber experiments. The fact that models are fundamentally limited by laboratory constraints also means that model results should be interpreted with the limitations of chamber experiments in mind. The work presented here indicates that some atmospheric RO_2 fate distributions can be better represented in chambers than others. For example, achieving τ_{bi} that allows for the same competition between bimolecular and unimolecular RO_2 reactions as what occurs in the atmosphere is most challenging for low-β environments, but can be reasonably well-captured under more polluted high-β conditions. As such, interpretation of model results, and their ability to reproduce field observations, should be done with awareness of the relevant RO_2 chemical environment.

Experimental chamber work over the last several decades has advanced our understanding of the complexity of the multi-generation oxidative chemistry involved in VOC oxidation and SOA production. To achieve the ultimate goal of fully understanding the processes that control the spatiotemporal distribution of pollutants in the atmosphere, the next generation of chamber studies must be more tightly connected to true atmospheric reaction conditions of RO_2 radicals. Such studies are the essential foundation for interpreting past and future field observations, and for building the accurate model parameterizations that are required to fully understand and predict atmospheric SOA, and ultimately its impacts on air quality and climate.

Materials and Methods

Modeling

We use the GEOS-Chem chemical transport model (version 13.4.0) at a horizontal grid resolution of 2°x2.5° and with 47 vertical layers. Results shown are from simulations of January and July 2016 after a 1-year spin-up with output saved every hour. The model is driven by assimilated meteorology from the Modern-Era Retrospective analysis for Research and Applications, Version 2 (MERRA-2), from the NASA Global Modeling and Assimilation Office (GMAO). Our simulations use the full gas-phase chemistry available in GEOS-Chem, including a coupled HO_x-NO_x-VOC-O_3-halogen chemical mechanism (*77–80*). Biogenic emissions are calculated online using the MEGANv2.1 framework (*81*) and anthropogenic emissions are from the global CEDS inventory (*82*).

Box model simulations were run using the Framework for 0D Atmospheric Modeling (F0AM) (*68*) with near-explicit chemistry described by the Master Chemical Mechanism (MCM v3.3.1) (*69*, *70*). Our simulations use a measured light spectrum scaled by a measured j_{NO2} rate of 0.12 min^{-1}. In order to span possible chamber initial conditions, we run a series of 8-hour simulations where we logarithmically permute initial isoprene (4 values between 0.1 and 100 ppb, inclusive, shown in Figure S7), HONO (18 values between 0 and 1,000 ppb, inclusive), H_2O_2 (12 values between 10 and 10,000 ppb, inclusive), and NO (18 values between 0 and 1,000 ppb, inclusive) concentrations that vary over orders of magnitude (Figures 5 and S8). We run a separate series of simulations where we permute initial CH_3ONO and NO concentrations (Figure S8). We consider a simulation in which the final methyl vinyl ketone (MVK) concentration is less than half of the maximum MVK concentration as an experiment that achieved second generation oxidation chemistry. For each simulation, we calculate β, τ_{bi}, RO_2/HO_2 and NO/NO_2. For experiments that achieve second-generation chemistry, the experiment end is defined as the time at which the MVK concentration decreases to half of its maximum. Other experiments are assumed to end at 8 hours. β is calculated from the cumulative integrated rates of RO_2 loss over the course of the experiment; $\tau_{bi,}$ RO_2/HO_2, and NO/NO_2 are calculated from the mean value during the simulated experiment.

Chamber experiments

Experiments were conducted in a 7.5 m^3 temperature-controlled environmental chamber (*71*) held at 20°C and RH < 10%. The chamber is constructed of PFA Teflon and is surrounded by 48 UV lamps whose emission is centered at 340 nm and whose intensity drives NO_2 photolysis at a rate of 0.12 min^{-1}. The chamber is operated in 'semi-batch' mode in which clean air is continuously added to make up for instrument sample flow to maintain a constant volume. Between experiments, the chamber is flushed by zero air for at least 12 h to ensure a clean background. Prior to the start of each experiment, ammonium sulfate seed particles are injected to serve as condensation nuclei, followed by injection of acetonitrile (dilution tracer), isoprene, and the oxidant precursors (HONO and/or H_2O_2). Seed particles are atomized from a 2 g/L solution of ammonium sulfate in water.

Isoprene and H_2O_2 are added through a silicone septum into a 10 lpm flow. HONO is generated by adding sulfuric acid via a syringe to a constantly stirred solution of sodium nitrite; the HONO produced, as well as any NO and NO_2 produced as co-products, are carried into the chamber via a 1 lpm air stream. Experiments are initiated by turning on the chamber lights.

The gas-phase composition of the reaction mixture was monitored with a proton-transfer-reaction time-of-flight mass spectrometer (Vocus PTR-MS, Aerodyne Research Inc.) (*83*) and an ammonium time-of-flight chemical ionization mass spectrometer (NH_4^+ CIMS, Ionicon Analytic) (*84*). Though not discussed here, particle-phase measurements were also made with an aerosol mass spectrometer (AMS, Aerodyne Research Inc.) and a scanning mobility particle sizer (TSI). Additional measurements include those from a NO-NO_2-NO_x analyzer (Thermo Scientific), a Cavity Attenuated Phase Shift Spectroscopy NO_2 monitor (CAPS NO_2) (Aerodyne Research Inc.), and an ozone monitor (2B Technologies).

Parameters that describe RO_2 fate (β, τ_{bi}, RO_2/HO_2, and NO/NO_2) for these experiments are calculated using MCM v3.3.1 box model simulations in F0AM as described above. Simulations are initialized with initial measured NO (from the NO channel of the Thermo Scientific NO-NO_2-NO_x analyzer), NO_2 (from the CAPS NO_2 monitor), HONO (estimated by subtracting the CAPS NO_2 signal from the NO_x analyzer NO_2 signal), and isoprene concentrations (from the Vocus PTR-MS). Initial H_2O_2 concentrations were estimated based on injection amount.

References

1. R. Burnett, H. Chen, M. Szyszkowicz, N. Fann, B. Hubbell, C. A. Pope, J. S. Apte, M. Brauer, A. Cohen, S. Weichenthal, J. Coggins, Q. Di, B. Brunekreef, J. Frostad, S. S. Lim, H. Kan, K. D. Walker, G. D. Thurston, R. B. Hayes, C. C. Lim, M. C. Turner, M. Jerrett, D. Krewski, S. M. Gapstur, W. R. Diver, B. Ostro, D. Goldberg, D. L. Crouse, R. V. Martin, P. Peters, L. Pinault, M. Tjepkema, A. van Donkelaar, P. J. Villeneuve, A. B. Miller, P. Yin, M. Zhou, L. Wang, N. A. H. Janssen, M. Marra, R. W. Atkinson, H. Tsang, T. Quoc Thach, J. B. Cannon, R. T. Allen, J. E. Hart, F. Laden, G. Cesaroni, F. Forastiere, G. Weinmayr, A. Jaensch, G. Nagel, H. Concin, J. V. Spadaro, Global estimates of mortality associated with long-term exposure to outdoor fine particulate matter. *Proceedings of the National Academy of Sciences* **115**, 9592–9597 (2018).

2. C. J. L. Murray, A. Y. Aravkin, P. Zheng, C. Abbafati, K. M. Abbas, M. Abbasi-Kangevari, F. Abd-Allah, A. Abdelalim, M. Abdollahi, I. Abdollahpour, K. H. Abegaz, H. Abolhassani, V. Aboyans, L. G. Abreu, M. R. M. Abrigo, A. Abualhasan, L. J. Abu-Raddad, A. I. Abushouk, M. Adabi, V. Adekanmbi, A. M. Adeoye, O. O. Adetokunboh, D. Adham, S. M. Advani, G. Agarwal, S. M. K. Aghamir, A. Agrawal, T. Ahmad, K. Ahmadi, M. Ahmadi, H. Ahmadieh, M. B. Ahmed, T. Y. Akalu, R. O. Akinyemi, T. Akinyemiju, B. Akombi, C. J. Akunna, F. Alahdab, Z. Al-Aly, K. Alam, S. Alam, T. Alam, F. M. Alanezi, T. M. Alanzi, B. wassihun Alemu, K. F. Alhabib, M. Ali, S. Ali, G. Alicandro, C. Alinia, V. Alipour, H. Alizade, S. M. Aljunid, F. Alla, P. Allebeck, A. Almasi-Hashiani, H. M. Al-Mekhlafi, J. Alonso, K. A. Altirkawi, M. Amini-Rarani, F. Amiri, D. A. Amugsi, R. Ancuceanu, D. Anderlini, J. A. Anderson, C. L. Andrei, T. Andrei, C. Angus, M. Anjomshoa, F. Ansari, A. Ansari-Moghaddam, I. C. Antonazzo, C. A. T. Antonio, C. M. Antony, E. Antriyandarti, D. Anvari, R. Anwer, S. C. Y. Appiah, J. Arabloo, M. Arab-Zozani, F. Ariani, B. Armoon, J. Ärnlöv, A. Arzani, M. Asadi-Aliabadi, A. A. Asadi-Pooya, C. Ashbaugh, M. Assmus, Z. Atafar, D. D. Atnafu, M. M. W. Atout, F. Ausloos, M. Ausloos, B. P. A. Quintanilla, G. Ayano, M. A. Ayanore, S. Azari, G. Azarian, Z. N. Azene, A. Badawi, A. D. Badiye, M. A. Bahrami, M. H. Bakhshaei, A. Bakhtiari, S. M. Bakkannavar, A. Baldasseroni, K. Ball, S. H.

Ballew, D. Balzi, M. Banach, S. K. Banerjee, A. B. Bante, A. G. Baraki, S. L. Barker-Collo, T. W. Bärnighausen, L. H. Barrero, C. M. Barthelemy, L. Barua, S. Basu, B. T. Baune, M. Bayati, J. S. Becker, N. Bedi, E. Beghi, Y. Béjot, M. L. Bell, F. B. Bennitt, I. M. Bensenor, K. Berhe, A. E. Berman, A. S. Bhagavathula, R. Bhageerathy, N. Bhala, D. Bhandari, K. Bhattacharyya, Z. A. Bhutta, A. Bijani, B. Bikbov, M. S. B. Sayeed, A. Biondi, B. M. Birihane, C. Bisignano, R. K. Biswas, H. Bitew, S. Bohlouli, M. Bohluli, A. S. Boon-Dooley, G. Borges, A. M. Borzì, S. Borzouei, C. Bosetti, S. Boufous, D. Braithwaite, N. J. K. Breitborde, S. Breitner, H. Brenner, P. S. Briant, A. N. Briko, N. I. Briko, G. B. Britton, D. Bryazka, B. R. Bumgarner, K. Burkart, R. T. Burnett, S. B. Nagaraja, Z. A. Butt, F. L. C. dos Santos, L. E. Cahill, L. L. A. Cámera, I. R. Campos-Nonato, R. Cárdenas, G. Carreras, J. J. Carrero, F. Carvalho, J. M. Castaldelli-Maia, C. A. Castañeda-Orjuela, G. Castelpietra, F. Castro, K. Causey, C. R. Cederroth, K. M. Cercy, E. Cerin, J. S. Chandan, K.-L. Chang, F. J. Charlson, V. K. Chattu, S. Chaturvedi, N. Cherbuin, O. Chimed-Ochir, D. Y. Cho, J.-Y. J. Choi, H. Christensen, D.-T. Chu, M. T. Chung, S.-C. Chung, F. M. Cicuttini, L. G. Ciobanu, M. Cirillo, T. K. D. Classen, A. J. Cohen, K. Compton, O. R. Cooper, V. M. Costa, E. Cousin, R. G. Cowden, D. H. Cross, J. A. Cruz, S. M. A. Dahlawi, A. A. M. Damasceno, G. Damiani, L. Dandona, R. Dandona, W. J. Dangel, A.-K. Danielsson, P. I. Dargan, A. M. Darwesh, A. Daryani, J. K. Das, R. D. Gupta, J. das Neves, C. A. Dávila-Cervantes, D. V. Davitoiu, D. D. Leo, L. Degenhardt, M. DeLang, R. P. Dellavalle, F. M. Demeke, G. T. Demoz, D. G. Demsie, E. Denova-Gutiérrez, N. Dervenis, G. P. Dhungana, M. Dianatinasab, D. D. da Silva, D. Diaz, Z. S. D. Forooshani, S. Djalalinia, H. T. Do, K. Dokova, F. Dorostkar, L. Doshmangir, T. R. Driscoll, B. B. Duncan, A. R. Duraes, A. W. Eagan, D. Edvardsson, N. E. Nahas, I. E. Sayed, M. E. Tantawi, I. Elbarazi, I. Y. Elgendy, S. I. El-Jaafary, I. R. Elyazar, S. Emmons-Bell, H. E. Erskine, S. Eskandarieh, S. Esmaeilnejad, A. Esteghamati, K. Estep, A. Etemadi, A. E. Etisso, J. Fanzo, M. Farahmand, M. Fareed, R. Faridnia, A. Farioli, A. Faro, M. Faruque, F. Farzadfar, N. Fattahi, M. Fazlzadeh, V. L. Feigin, R. Feldman, S.-M. Fereshtehnejad, E. Fernandes, G. Ferrara, A. J. Ferrari, M. L. Ferreira, I. Filip, F. Fischer, J. L. Fisher, L. S. Flor, N. A. Foigt, M. O. Folayan, A. A. Fomenkov, L. M. Force, M. Foroutan, R. C. Franklin, M. Freitas, W. Fu, T. Fukumoto, J. M. Furtado, M. M. Gad, E. Gakidou, S. Gallus, A. L. Garcia-Basteiro, W. M. Gardner, B. S. Geberemariyam, A. A. A. A. Gebreslassie, A. Geremew, A. G. Hayoon, P. W. Gething, M. Ghadimi, K. Ghadiri, F. Ghaffarifar, M. Ghafourifard, F. Ghamari, A. Ghashghaee, H. Ghiasvand, N. Ghith, A. Gholamian, R. Ghosh, P. S. Gill, T. G. G. Ginindza, G. Giussani, E. V. Gnedovskaya, S. Goharinezhad, S. V. Gopalani, G. Gorini, H. Goudarzi, A. C. Goulart, F. Greaves, M. Grivna, G. Grosso, M. I. M. Gubari, H. C. Gugnani, R. A. Guimarães, R. A. Guled, G. Guo, Y. Guo, R. Gupta, T. Gupta, B. Haddock, N. Hafezi-Nejad, A. Hafiz, A. Haj-Mirzaian, A. Haj-Mirzaian, B. J. Hall, I. Halvaei, R. R. Hamadeh, S. Hamidi, M. S. Hammer, G. J. Hankey, H. Haririan, J. M. Haro, A. I. Hasaballah, M. M. Hasan, E. Hasanpoor, A. Hashi, S. Hassanipour, H. Hassankhani, R. J. Havmoeller, S. I. Hay, K. Hayat, G. Heidari, R. Heidari-Soureshjani, H. J. Henrikson, M. E. Herbert, C. Herteliu, F. Heydarpour, T. R. Hird, H. W. Hoek, R. Holla, P. Hoogar, H. D. Hosgood, N. Hossain, M. Hosseini, M. Hosseinzadeh, M. Hostiuc, S. Hostiuc, M. Househ, M. Hsairi, V. C. Hsieh, G. Hu, K. Hu, T. M. Huda, A. Humayun, C. K. Huynh, B.-F. Hwang, V. C. Iannucci, S. E. Ibitoye, N. Ikeda, K. S. Ikuta, O. S. Ilesanmi, I. M. Ilic, M. D. Ilic, L. R. Inbaraj, H. Ippolito, U. Iqbal, S. S. N. Irvani, C. M. S. Irvine, M. M. Islam, S. M. S. Islam, H. Iso, R. Q. Ivers, C. C. D. Iwu, C. J. Iwu, I. O. Iyamu, J. Jaafari, K. H. Jacobsen, H. Jafari, M. Jafarinia, M. A. Jahani, M. Jakovljevic, F. Jalilian, S. L. James, H. Janjani, T. Javaheri, J. Javidnia, P. Jeemon, E. Jenabi, R. P. Jha, V. Jha, J. S. Ji, L. Johansson, O. John, Y. O. John-Akinola, C. O. Johnson, J. B. Jonas, F. Joukar, J. J. Jozwiak, M. Jürisson, A. Kabir, Z. Kabir, H. Kalani, R. Kalani, L. R. Kalankesh, R. Kalhor, T. Kanchan, N. Kapoor, B. K. Matin, A. Karch, M.

A. Karim, G. M. Kassa, S. V. Katikireddi, G. A. Kayode, A. K. Karyani, P. N. Keiyoro, C. Keller, L. Kemmer, P. J. Kendrick, N. Khalid, M. Khammarnia, E. A. Khan, M. Khan, K. Khatab, M. M. Khater, M. N. Khatib, M. Khayamzadeh, S. Khazaei, C. Kieling, Y. J. Kim, R. W. Kimokoti, A. Kisa, S. Kisa, M. Kivimäki, L. D. Knibbs, A. K. S. Knudsen, J. M. Kocarnik, S. Kochhar, J. A. Kopec, V. A. Korshunov, P. A. Koul, A. Koyanagi, M. U. G. Kraemer, K. Krishan, K. J. Krohn, H. Kromhout, B. K. Defo, G. A. Kumar, V. Kumar, O. P. Kurmi, D. Kusuma, C. L. Vecchia, B. Lacey, D. K. Lal, R. Lalloo, T. Lallukka, F. H. Lami, I. Landires, J. J. Lang, S. M. Langan, A. O. Larsson, S. Lasrado, P. Lauriola, J. V. Lazarus, P. H. Lee, S. W. H. Lee, K. E. LeGrand, J. Leigh, M. Leonardi, H. Lescinsky, J. Leung, M. Levi, S. Li, L.-L. Lim, S. Linn, S. Liu, S. Liu, Y. Liu, J. Lo, A. D. Lopez, J. C. F. Lopez, P. D. Lopukhov, S. Lorkowski, P. A. Lotufo, A. Lu, A. Lugo, E. R. Maddison, P. W. Mahasha, M. M. Mahdavi, M. Mahmoudi, A. Majeed, A. Maleki, S. Maleki, R. Malekzadeh, D. C. Malta, A. A. Mamun, A. L. Manda, H. Manguerra, F. Mansour-Ghanaei, B. Mansouri, M. A. Mansournia, A. M. M. Herrera, J. C. Maravilla, A. Marks, R. V. Martin, S. Martini, F. R. Martins-Melo, A. Masaka, S. Z. Masoumi, M. R. Mathur, K. Matsushita, P. K. Maulik, C. McAlinden, J. J. McGrath, M. McKee, M. M. Mehndiratta, F. Mehri, K. M. Mehta, Z. A. Memish, W. Mendoza, R. G. Menezes, E. W. Mengesha, A. Mereke, S. T. Mereta, A. Meretoja, T. J. Meretoja, T. Mestrovic, B. Miazgowski, T. Miazgowski, I. M. Michalek, T. R. Miller, E. J. Mills, G. K. Mini, M. Miri, A. Mirica, E. M. Mirrakhimov, H. Mirzaei, M. Mirzaei, R. Mirzaei, M. Mirzaei-Alavijeh, A. T. Misganaw, P. Mithra, B. Moazen, D. K. Mohammad, Y. Mohammad, N. M. G. Mezerji, A. Mohammadian-Hafshejani, N. Mohammadifard, R. Mohammadpourhodki, A. S. Mohammed, H. Mohammed, J. A. Mohammed, S. Mohammed, A. H. Mokdad, M. Molokhia, L. Monasta, M. D. Mooney, G. Moradi, M. Moradi, M. Moradi-Lakeh, R. Moradzadeh, P. Moraga, L. Morawska, J. Morgado-da-Costa, S. D. Morrison, A. Mosapour, J. F. Mosser, S. Mouodi, S. M. Mousavi, A. M. Khaneghah, U. O. Mueller, S. Mukhopadhyay, E. C. Mullany, K. I. Musa, S. Muthupandian, A. F. Nabhan, M. Naderi, A. J. Nagarajan, G. Nagel, M. Naghavi, B. Naghshtabrizi, M. D. Naimzada, F. Najafi, V. Nangia, J. R. Nansseu, M. Naserbakht, V. C. Nayak, I. Negoi, J. W. Ngunjiri, C. T. Nguyen, H. L. T. Nguyen, M. Nguyen, Y. T. Nigatu, R. Nikbakhsh, M. R. Nixon, C. A. Nnaji, S. Nomura, B. Norrving, J. J. Noubiap, C. Nowak, V. Nunez-Samudio, A. Oţoiu, B. Oancea, C. M. Odell, F. A. Ogbo, I.-H. Oh, E. W. Okunga, M. Oladnabi, A. T. Olagunju, B. O. Olusanya, J. O. Olusanya, M. O. Omer, K. L. Ong, O. E. Onwujekwe, H. M. Orpana, A. Ortiz, O. Osarenotor, F. B. Osei, S. M. Ostroff, N. Otstavnov, S. S. Otstavnov, S. Øverland, M. O. Owolabi, M. P. A, J. R. Padubidri, R. Palladino, S. Panda-Jonas, A. Pandey, C. D. H. Parry, M. Pasovic, D. K. Pasupula, S. K. Patel, M. Pathak, S. B. Patten, G. C. Patton, H. P. Toroudi, A. E. Peden, A. Pennini, V. C. F. Pepito, E. K. Peprah, D. M. Pereira, K. Pesudovs, H. Q. Pham, M. R. Phillips, C. Piccinelli, T. M. Pilz, M. A. Piradov, M. Pirsaheb, D. Plass, S. Polinder, K. R. Polkinghorne, C. D. Pond, M. J. Postma, H. Pourjafar, F. Pourmalek, A. Poznańska, S. I. Prada, V. Prakash, D. R. A. Pribadi, E. Pupillo, Z. Q. Syed, M. Rabiee, N. Rabiee, A. Radfar, A. Rafiee, A. Raggi, M. A. Rahman, A. Rajabpour-Sanati, F. Rajati, I. Rakovac, P. Ram, K. Ramezanzadeh, C. L. Ranabhat, P. C. Rao, S. J. Rao, V. Rashedi, P. Rathi, D. L. Rawaf, S. Rawaf, L. Rawal, R. Rawassizadeh, R. Rawat, C. Razo, S. B. Redford, R. C. Reiner, M. B. Reitsma, G. Remuzzi, V. Renjith, A. M. N. Renzaho, S. Resnikoff, N. Rezaei, N. Rezaei, A. Rezapour, P.-A. Rhinehart, S. M. Riahi, D. C. Ribeiro, D. Ribeiro, J. Rickard, J. A. Rivera, N. L. S. Roberts, S. Rodríguez-Ramírez, L. Roever, L. Ronfani, R. Room, G. Roshandel, G. A. Roth, D. Rothenbacher, E. Rubagotti, G. M. Rwegerera, S. Sabour, P. S. Sachdev, B. Saddik, E. Sadeghi, M. Sadeghi, R. Saeedi, S. S. Moghaddam, Y. Safari, S. Safi, S. Safiri, R. Sagar, A. Sahebkar, S. M. Sajadi, N. Salam, P. Salamati, H. Salem, M. R. R. Salem, H. Salimzadeh, O. M. Salman, J. A. Salomon, Z. Samad, H. S. Kafil, E. Z. Sambala, A. M. Samy, J. Sanabria,

T. G. Sánchez-Pimienta, D. F. Santomauro, I. S. Santos, J. V. Santos, M. M. Santric-Milicevic, S. Y. I. Saraswathy, R. Sarmiento-Suárez, N. Sarrafzadegan, B. Sartorius, A. Sarveazad, B. Sathian, T. Sathish, D. Sattin, S. Saxena, L. E. Schaeffer, S. Schiavolin, M. P. Schlaich, M. I. Schmidt, A. E. Schutte, D. C. Schwebel, F. Schwendicke, A. M. Senbeta, S. Senthilkumaran, S. G. Sepanlou, B. Serdar, M. L. Serre, J. Shadid, O. Shafaat, S. Shahabi, A. A. Shaheen, M. A. Shaikh, A. S. Shalash, M. Shams-Beyranvand, M. Shamsizadeh, K. Sharafi, A. Sheikh, A. Sheikhtaheri, K. Shibuya, K. D. Shield, M. Shigematsu, J. I. Shin, M.-J. Shin, R. Shiri, R. Shirkoohi, K. Shuval, S. Siabani, R. Sierpinski, I. D. Sigfusdottir, R. Sigurvinsdottir, J. P. Silva, K. E. Simpson, J. A. Singh, P. Singh, E. Skiadaresi, S. T. Skou, V. Y. Skryabin, E. U. R. Smith, A. Soheili, S. Soltani, M. Soofi, R. J. D. Sorensen, J. B. Soriano, M. B. Sorrie, S. Soshnikov, I. N. Soyiri, C. N. Spencer, A. Spotin, C. T. Sreeramareddy, V. Srinivasan, J. D. Stanaway, C. Stein, D. J. Stein, C. Steiner, L. Stockfelt, M. A. Stokes, K. Straif, J. L. Stubbs, M. B. Sufiyan, H. A. R. Suleria, R. S. Abdulkader, G. Sulo, I. Sultan, Ł. Szumowski, R. Tabarés-Seisdedos, K. M. Tabb, T. Tabuchi, A. Taherkhani, M. Tajdini, K. Takahashi, J. S. Takala, A. T. Tamiru, N. Taveira, A. Tehrani-Banihashemi, M.-H. Temsah, G. A. Tesema, Z. T. Tessema, G. D. Thurston, M. V. Titova, H. R. Tohidinik, M. Tonelli, R. Topor-Madry, F. Topouzis, A. E. Torre, M. Touvier, M. R. R. Tovani-Palone, B. X. Tran, R. Travillian, A. Tsatsakis, L. T. Car, S. Tyrovolas, R. Uddin, C. D. Umeokonkwo, B. Unnikrishnan, E. Upadhyay, M. Vacante, P. R. Valdez, A. van Donkelaar, T. J. Vasankari, Y. Vasseghian, Y. Veisani, N. Venketasubramanian, F. S. Violante, V. Vlassov, S. E. Vollset, T. Vos, R. Vukovic, Y. Waheed, M. T. Wallin, Y. Wang, Y.-P. Wang, A. Watson, J. Wei, M. Y. W. Wei, R. G. Weintraub, J. Weiss, A. Werdecker, J. J. West, R. Westerman, J. L. Whisnant, H. A. Whiteford, K. E. Wiens, C. D. A. Wolfe, S. S. Wozniak, A.-M. Wu, J. Wu, S. W. Hanson, G. Xu, R. Xu, S. Yadgir, S. H. Y. Jabbari, K. Yamagishi, M. Yaminfirooz, Y. Yano, S. Yaya, V. Yazdi-Feyzabadi, T. Y. Yeheyis, C. S. Yilgwan, M. T. Yilma, P. Yip, N. Yonemoto, M. Z. Younis, T. P. Younker, B. Yousefi, Z. Yousefi, T. Yousefinezhadi, A. Y. Yousuf, C. Yu, H. Yusefzadeh, T. Z. Moghadam, M. Zamani, M. Zamanian, H. Zandian, M. S. Zastrozhin, Y. Zhang, Z.-J. Zhang, J. T. Zhao, X.-J. G. Zhao, Y. Zhao, M. Zhou, A. Ziapour, S. R. M. Zimsen, M. Brauer, A. Afshin, S. S. Lim, Global burden of 87 risk factors in 204 countries and territories, 1990–2019: a systematic analysis for the Global Burden of Disease Study 2019. *The Lancet* **396**, 1223–1249 (2020).

3. IPCC, "Climate Change 2021: The Physical Science Basis. Contribution of Working Group I to the Sixth Assessment Report of the Intergovernmental Panel on Climate Change" (Cambridge University Press, Cambridge, United Kingdom and New York, NY, USA, 2021); 10.1017/9781009157896.

4. Q. Zhang, J. L. Jimenez, M. R. Canagaratna, J. D. Allan, H. Coe, I. Ulbrich, M. R. Alfarra, A. Takami, A. M. Middlebrook, Y. L. Sun, K. Dzepina, E. Dunlea, K. Docherty, P. F. Decarlo, D. Salcedo, T. Onasch, J. T. Jayne, T. Miyoshi, A. Shimono, S. Hatakeyama, N. Takegawa, Y. Kondo, J. Schneider, F. Drewnick, L. Cottrell, R. J. Griffin, J. Rautiainen, J. Y. Sun, Y. M. Zhang, Ubiquity and dominance of oxygenated species in organic aerosols in anthropogenically-influenced Northern Hemisphere midlatitudes. *Geophysical Research Letters* **34**, 1–6 (2007).

5. B. J. Turpin, J. J. Huntzicker, Identification of secondary organic aerosol episodes and quantitation of primary and secondary organic aerosol concentrations during SCAQS. *Atmospheric Environment* **29**, 3527–3544 (1995).

6. M. Shrivastava, C. D. Cappa, J. Fan, Allen. H. Goldstein, A. B. Guenther, J. L. Jimenez, C. Kuang, A. Laskin, S. T. Martin, N. L. Ng, T. Petaja, J. R. Pierce, P. J. Rasch, P. Roldin, J. H. Seinfeld, J. Shilling, J. N. Smith, J. A. Thornton, R. Volkamer, J. Wang, D. R. Worsnop, R. A. Zaveri, A. Zelenyuk, Q. Zhang, Recent advances in understanding secondary organic aerosol: Implications for global climate forcing. *Reviews of Geophysics* **55**, 509–559 (2017).

7. J. Tyndall, XIX. On the action of rays of high refrangibility upon gaseous matter. *Phil. Trans. R. Soc.* **160**, 333–365 (1870).

8. A. J. Haagen-Smit, Chemistry and physiology of Los Angeles smog. *Ind. Eng. Chem.; (United States)* **44:6** (1952).

9. F. W. Went, Blue Hazes in the Atmosphere. *Nature* **187**, 641–643 (1960).

10. R. M. Kamens, H. E. Jeffries, M. W. Gery, R. W. Wiener, K. G. Sexton, G. B. Howe, The impact of α-pinene on urban smog formation: an outdoor smog chamber study. *Atmospheric Environment (1967)* **15**, 969–981 (1981).

11. S. Hatakeyama, K. Izumi, T. Fukuyama, H. Akimoto, Reactions of ozone with α-pinene and β-pinene in air: Yields of gaseous and particulate products. *Journal of Geophysical Research: Atmospheres* **94**, 13013–13024 (1989).

12. K. Izumi, T. Fukuyama, Photochemical aerosol formation from aromatic hydrocarbons in the presence of NOx. *Atmospheric Environment. Part A. General Topics* **24**, 1433–1441 (1990).

13. S. E. Paulson, S. N. Pandis, U. Baltensperger, J. H. Seinfeld, R. C. Flagan, E. J. Palen, D. T. Allen, C. Schaffner, W. Giger, A. Portmann, Characterization of photochemical aerosols from biogenic hydrocarbons. *Journal of Aerosol Science* **21**, S245–S248 (1990).

14. S. N. Pandis, S. E. Paulson, J. H. Seinfeld, R. C. Flagan, Aerosol formation in the photooxidation of isoprene and β-pinene. *Atmospheric Environment. Part A. General Topics* **25**, 997–1008 (1991).

15. S. Hatakeyama, K. Izumi, T. Fukuyama, H. Akimoto, N. Washida, Reactions of OH with α-pinene and β-pinene in air: Estimate of global CO production from the atmospheric oxidation of terpenes. *Journal of Geophysical Research: Atmospheres* **96**, 947–958 (1991).

16. S.-H. Zhang, M. Shaw, J. H. Seinfeld, R. C. Flagan, Photochemical aerosol formation from α-pinene- and β-pinene. *Journal of Geophysical Research: Atmospheres* (1992).

17. T. Hoffmann, J. R. Odum, F. Bowman, D. Collins, D. Klockow, R. C. Flagan, J. H. Seinfeld, Formation of Organic Aerosols from the Oxidation of Biogenic Hydrocarbons. *Journal of Atmospheric Chemistry* **26**, 189–222 (1997).

18. R. J. Griffin, D. R. Cocker III, R. C. Flagan, J. H. Seinfeld, Organic aerosol formation from the oxidation of biogenic hydrocarbons. *Journal of Geophysical Research: Atmospheres* **104**, 3555–3567 (1999).

19. S. N. Pandis, R. A. Harley, G. R. Cass, J. H. Seinfeld, Secondary organic aerosol formation and transport. *Atmospheric Environment. Part A. General Topics* **26**, 2269–2282 (1992).

20. S. H. Chung, J. H. Seinfeld, Global distribution and climate forcing of carbonaceous aerosols. *Journal of Geophysical Research: Atmospheres* **107**, AAC 14-1-AAC 14-33 (2002).

21. K. Tsigaridis, M. Kanakidou, Global modelling of secondary organic aerosol in the troposphere: a sensitivity analysis. *Atmospheric Chemistry and Physics* **3**, 1849–1869 (2003).

22. C. Song, K. Na, D. R. Cocker, Impact of the Hydrocarbon to NO_x Ratio on Secondary Organic Aerosol Formation. *Environ. Sci. Technol.* **39**, 3143–3149 (2005).

23. K. S. Docherty, P. J. Ziemann, Effects of Stabilized Criegee Intermediate and OH Radical Scavengers on Aerosol Formation from Reactions of β-Pinene with O_3. *Aerosol Science and Technology* **37**, 877–891 (2003).

24. D. Johnson, M. E. Jenkin, K. Wirtz, M. Martin-Reviejo, D. Johnson, M. E. Jenkin, K. Wirtz, M. Martin-Reviejo, Simulating the Formation of Secondary Organic Aerosol from the Photooxidation of Toluene. *Environ. Chem.* **1**, 150–165 (2004).

25. K. S. Docherty, W. Wu, Y. B. Lim, P. J. Ziemann, Contributions of Organic Peroxides to Secondary Aerosol Formed from Reactions of Monoterpenes with O_3. *Environ. Sci. Technol.* **39**, 4049–4059 (2005).

26. A. A. Presto, K. E. Huff Hartz, N. M. Donahue, Secondary Organic Aerosol Production from Terpene Ozonolysis. 2. Effect of NO_x Concentration. *Environ. Sci. Technol.* **39**, 7046–7054 (2005).

27. J. H. Kroll, N. L. Ng, S. M. Murphy, R. C. Flagan, J. H. Seinfeld, Secondary Organic Aerosol Formation from Isoprene Photooxidation. *Environ. Sci. Technol.* **40**, 1869–1877 (2006).

28. M. Martín-Reviejo, K. Wirtz, Is Benzene a Precursor for Secondary Organic Aerosol? *Environ. Sci. Technol.* **39**, 1045–1054 (2005).

29. J. H. Kroll, N. L. Ng, S. M. Murphy, R. C. Flagan, J. H. Seinfeld, Secondary organic aerosol formation from isoprene photooxidation under high-NO_x conditions. *Geophysical Research Letters* **32** (2005).

30. N. L. Ng, P. S. Chhabra, A. W. H. Chan, J. D. Surratt, J. H. Kroll, A. J. Kwan, D. C. McCabe, P. O. Wennberg, A. Sorooshian, S. M. Murphy, N. F. Dalleska, R. C. Flagan, J. H. Seinfeld, Effect of NO_x level on secondary organic aerosol (SOA) formation from the photooxidation of terpenes. *Atmospheric Chemistry and Physics* **7**, 5159–5174 (2007).

31. N. L. Ng, J. H. Kroll, A. W. H. Chan, P. S. Chhabra, R. C. Flagan, J. H. Seinfeld, Secondary organic aerosol formation from *m*-xylene, toluene, and benzene. *Atmospheric Chemistry and Physics* **7**, 3909–3922 (2007).

32. C. Song, K. Na, B. Warren, Q. Malloy, D. R. Cocker, Secondary Organic Aerosol Formation from m-Xylene in the Absence of NO_x. *Environ. Sci. Technol.* **41**, 7409–7416 (2007).

33. H. O. T. Pye, A. W. H. Chan, M. P. Barkley, J. H. Seinfeld, Global modeling of organic aerosol: The importance of reactive nitrogen (NO_x and NO_3). *Atmospheric Chemistry and Physics* **10**, 11261–11276 (2010).

34. A. A. Presto, N. M. Donahue, Investigation of α-Pinene + Ozone Secondary Organic Aerosol Formation at Low Total Aerosol Mass. *Environ. Sci. Technol.* **40**, 3536–3543 (2006).

35. J. Zhang, K. E. Huff Hartz, S. N. Pandis, N. M. Donahue, Secondary Organic Aerosol Formation from Limonene Ozonolysis: Homogeneous and Heterogeneous Influences as a Function of NO_x. *J. Phys. Chem. A* **110**, 11053–11063 (2006).

36. D. K. Henze, J. H. Seinfeld, Global secondary organic aerosol from isoprene oxidation. *Geophysical Research Letters* **33** (2006).

37. D. K. Henze, J. H. Seinfeld, N. L. Ng, J. H. Kroll, T.-M. Fu, D. J. Jacob, C. L. Heald, Global modeling of secondary organic aerosol formation from aromatic hydrocarbons: high- vs. low-yield pathways. *Atmospheric Chemistry and Physics* **8**, 2405–2420 (2008).

38. C. L. Heald, D. K. Henze, L. W. Horowitz, J. Feddema, J. F. Lamarque, A. Guenther, P. G. Hess, F. Vitt, J. H. Seinfeld, A. H. Goldstein, I. Fung, Predicted change in global secondary organic aerosol concentrations in response to future climate, emissions, and land use change. *Journal of Geophysical Research Atmospheres*, doi: https://doi.org/10.1029/2007JD009092 (2008).

39. J. Peeters, J.-F. Muller, HO_x radical regeneration in isoprene oxidation via peroxy radical isomerisations. II : experimental evidence and global impact. *Physical Chemistry Chemical Physics* **12**, 14227–14235 (2010).

40. J. D. Crounse, L. B. Nielsen, S. Jørgensen, H. G. Kjaergaard, P. O. Wennberg, Autoxidation of organic compounds in the atmosphere. *Journal of Physical Chemistry Letters* **4**, 3513–3520 (2013).

41. M. Ehn, J. A. Thornton, E. Kleist, M. Sipilä, H. Junninen, I. Pullinen, M. Springer, F. Rubach, R. Tillmann, B. Lee, F. Lopez-Hilfiker, S. Andres, I. H. Acir, M. Rissanen, T. Jokinen, S. Schobesberger, J. Kangasluoma, J. Kontkanen, T. Nieminen, T. Kurtén, L. B. Nielsen, S. Jørgensen, H. G. Kjaergaard, M. Canagaratna, M. D. Maso, T. Berndt, T. Petäjä, A. Wahner, V. M. Kerminen, M. Kulmala, D. R. Worsnop, J. Wildt, T. F. Mentel, A large source of low-volatility secondary organic aerosol. *Nature* **506**, 476–479 (2014).

42. M. P. Rissanen, NO2 Suppression of Autoxidation–Inhibition of Gas-Phase Highly Oxidized Dimer Product Formation. *ACS Earth Space Chem.* **2**, 1211–1219 (2018).

43. K. J. Nihill, Q. Ye, F. Majluf, J. E. Krechmer, M. R. Canagaratna, J. H. Kroll, Influence of the NO/NO_2 Ratio on Oxidation Product Distributions under High-NO Conditions. *Environ. Sci. Technol.* **55**, 6594–6601 (2021).

44. A. W. H. Chan, M. N. Chan, J. D. Surratt, P. S. Chhabra, C. L. Loza, J. D. Crounse, L. D. Yee, R. C. Flagan, P. O. Wennberg, J. H. Seinfeld, Role of aldehyde chemistry and NO_x concentrations in secondary organic aerosol formation. *Atmospheric Chemistry and Physics* **10**, 7169–7188 (2010).

45. M. D. Keywood, J. H. Kroll, V. Varutbangkul, R. Bahreini, R. C. Flagan, J. H. Seinfeld, Secondary Organic Aerosol Formation from Cyclohexene Ozonolysis: Effect of OH Scavenger and the Role of Radical Chemistry. *Environ. Sci. Technol.* **38**, 3343–3350 (2004).

46. W. Peng, C. Le, W. C. Porter, D. R. I. Cocker, Variability in Aromatic Aerosol Yields under Very Low NO_x Conditions at Different HO_2/RO_2 Regimes. *Environ. Sci. Technol.* **56**, 750–760 (2022).

47. Y. Baker, S. Kang, H. Wang, R. Wu, J. Xu, A. Zanders, Q. He, T. Hohaus, T. Ziehm, V. Geretti, T. J. Bannan, S. P. O'Meara, A. Voliotis, M. Hallquist, G. McFiggans, S. R. Zorn, A. Wahner, T. Mentel, Impact of HO_2/RO_2 ratio on highly oxygenated α-pinene photooxidation products and secondary organic aerosol formation potential. *EGUsphere*, 1–32 (2023).

48. T. Berndt, W. Scholz, B. Mentler, L. Fischer, H. Herrmann, M. Kulmala, A. Hansel, Accretion Product Formation from Self- and Cross-Reactions of RO_2 Radicals in the Atmosphere. *Angewandte Chemie International Edition* **57**, 3820–3824 (2018).

49. Y. Zhao, J. A. Thornton, H. O. T. Pye, Quantitative constraints on autoxidation and dimer formation from direct probing of monoterpene-derived peroxy radical chemistry. *Proceedings of the National Academy of Sciences* **115**, 12142–12147 (2018).

50. G. McFiggans, T. F. Mentel, J. Wildt, I. Pullinen, S. Kang, E. Kleist, S. Schmitt, M. Springer, R. Tillmann, C. Wu, D. Zhao, M. Hallquist, C. Faxon, M. Le Breton, Å. M. Hallquist, D. Simpson, R. Bergström, M. E. Jenkin, M. Ehn, J. A. Thornton, M. R. Alfarra, T. J. Bannan, C. J. Percival, M. Priestley, D. Topping, A. Kiendler-Scharr, Secondary organic aerosol reduced by mixture of atmospheric vapours. *Nature* **565**, 587–593 (2019).

51. K. Tsigaridis, N. Daskalakis, M. Kanakidou, P. J. Adams, P. Artaxo, R. Bahadur, Y. Balkanski, S. E. Bauer, N. Bellouin, A. Benedetti, T. Bergman, T. K. Berntsen, J. P. Beukes, H. Bian, K. S. Carslaw, M. Chin, G. Curci, T. Diehl, R. C. Easter, S. J. Ghan, S. L. Gong, A. Hodzic, C. R. Hoyle, T. Iversen, S. Jathar, J. L. Jimenez, J. W. Kaiser, A. Kirkeväg, D. Koch, H. Kokkola, Y. H Lee, G. Lin, X. Liu, G. Luo, X. Ma, G. W. Mann, N. Mihalopoulos, J. J. Morcrette, J. F. Müller, G. Myhre, S. Myriokefalitakis, N. L. Ng, D. O'donnell, J. E. Penner, L. Pozzoli, K. J. Pringle, L. M. Russell, M. Schulz, J. Sciare, Seland, D. T. Shindell, S. Sillman, R. B. Skeie, D. Spracklen, T. Stavrakou, S. D. Steenrod, T. Takemura, P. Tiitta, S. Tilmes, H. Tost, T. Van Noije, P. G. Van Zyl, K. Von Salzen, F. Yu, Z. Wang, Z. Wang, R. A. Zaveri, H. Zhang, K. Zhang, Q. Zhang, X. Zhang, The AeroCom evaluation and intercomparison of organic aerosol in global models. *Atmospheric Chemistry and Physics* **14**, 10845–10895 (2014).

52. S. J. Pai, C. L. Heald, J. R. Pierce, S. C. Farina, E. A. Marais, J. L. Jimenez, P. Campuzano-Jost, B. A. Nault, A. M. Middlebrook, H. Coe, J. E. Shilling, R. Bahreini, J. H. Dingle, K. Vu, An evaluation of global organic aerosol schemes using airborne observations. *Atmospheric Chemistry and Physics* **20**, 2637–2665 (2020).

53. W. C. Porter, J. L. Jimenez, K. C. Barsanti, Quantifying Atmospheric Parameter Ranges for Ambient Secondary Organic Aerosol Formation. *ACS Earth Space Chem.* **5**, 2380–2397 (2021).

54. P. O. Wennberg, Let's Abandon the "High NO_x" and "Low NO_x" Terminology. *ACS EST Air*, doi: 10.1021/acsestair.3c00055 (2023).

55. A. P. Teng, J. D. Crounse, P. O. Wennberg, Isoprene Peroxy Radical Dynamics. *Journal of the American Chemical Society* **139**, 5367–5377 (2017).

56. M. Schervish, N. M. Donahue, Peroxy radical kinetics and new particle formation. *Environmental Science: Atmospheres* **1**, 79–92 (2021).

57. P. O. Wennberg, K. H. Bates, J. D. Crounse, L. G. Dodson, R. C. McVay, L. A. Mertens, T. B. Nguyen, E. Praske, R. H. Schwantes, M. D. Smarte, J. M. St Clair, A. P. Teng, X. Zhang, J. H. Seinfeld, Gas-Phase Reactions of Isoprene and Its Major Oxidation Products. *Chemical Reviews* **118**, 3337–3390 (2018).

58. E. Praske, R. V. Otkjær, J. D. Crounse, J. C. Hethcox, B. M. Stoltz, H. G. Kjaergaard, P. O. Wennberg, Atmospheric autoxidation is increasingly important in urban and suburban North America. *Proceedings of the National Academy of Sciences of the United States of America* **115**, 64–69 (2018).

59. L. Xu, K. H. Møller, J. D. Crounse, R. V. Otkjær, H. G. Kjaergaard, P. O. Wennberg, Unimolecular Reactions of Peroxy Radicals Formed in the Oxidation of α-Pinene and β-Pinene by Hydroxyl Radicals. *J. Phys. Chem. A* **123**, 1661–1674 (2019).

60. E. L. D'Ambro, B. H. Lee, J. Liu, J. E. Shilling, C. J. Gaston, F. D. Lopez-Hilfiker, S. Schobesberger, R. A. Zaveri, C. Mohr, A. Lutz, Z. Zhang, A. Gold, J. D. Surratt, J. C. Rivera-Rios, F. N. Keutsch, J. A. Thornton, Molecular composition and volatility of isoprene photochemical oxidation secondary organic aerosol under low- and high-NO_x conditions. *Atmospheric Chemistry and Physics* **17**, 159–174 (2017).

61. J. A. Thornton, J. E. Shilling, M. Shrivastava, E. L. D'Ambro, M. A. Zawadowicz, J. Liu, A Near-Explicit Mechanistic Evaluation of Isoprene Photochemical Secondary Organic Aerosol Formation and Evolution: Simulations of Multiple Chamber Experiments with and without Added NOx. *ACS Earth Space Chem.* **4**, 1161–1181 (2020).

62. J. E. Shilling, Q. Chen, S. M. King, T. Rosenoern, J. H. Kroll, D. R. Worsnop, K. A. McKinney, S. T. Martin, Particle mass yield in secondary organic aerosol formed by the dark ozonolysis of α-pinene. *Atmospheric Chemistry and Physics* **8**, 2073–2088 (2008).

63. W. Nie, C. Yan, L. Yang, P. Roldin, Y. Liu, A. L. Vogel, U. Molteni, D. Stolzenburg, H. Finkenzeller, A. Amorim, F. Bianchi, J. Curtius, L. Dada, D. C. Draper, J. Duplissy, A. Hansel, X.-C. He, V. Hofbauer, T. Jokinen, C. Kim, K. Lehtipalo, L. Nichman, R. L. Mauldin, V. Makhmutov, B. Mentler, A. Mizelli-Ojdanic, T. Petäjä, L. L. J. Quéléver, S. Schallhart, M. Simon, C. Tauber, A. Tomé, R. Volkamer, A. C. Wagner, R. Wagner, M. Wang, P. Ye, H. Li, W. Huang, X. Qi, S. Lou, T. Liu, X. Chi, J. Dommen, U. Baltensperger, I. El Haddad, J. Kirkby, D. Worsnop, M. Kulmala, N. M. Donahue, M. Ehn, A. Ding, NO at low concentration can enhance the formation of highly oxygenated biogenic molecules in the atmosphere. *Nat Commun* **14**, 3347 (2023).

64. A. Lambe, P. Massoli, X. Zhang, M. Canagaratna, J. Nowak, C. Daube, C. Yan, W. Nie, T. Onasch, J. Jayne, C. Kolb, P. Davidovits, D. Worsnop, W. Brune, Controlled nitric oxide production via $O(^1D) + N_2O$ reactions for use in oxidation flow reactor studies. *Atmospheric Measurement Techniques* **10**, 2283–2298 (2017).

65. Z. Peng, J. Lee-Taylor, J. J. Orlando, G. S. Tyndall, J. L. Jimenez, Organic peroxy radical chemistry in oxidation flow reactors and environmental chambers and their atmospheric relevance. *Atmospheric Chemistry and Physics* **19**, 813–834 (2019).

66. E. Ahlberg, A. Eriksson, W. H. Brune, P. Roldin, B. Svenningsson, Effect of salt seed particle surface area, composition and phase on secondary organic aerosol mass yields in oxidation flow reactors. *Atmospheric Chemistry and Physics* **19**, 2701–2712 (2019).

67. Z. Li, A. Buchholz, L. M. F. Barreira, A. Ylisirniö, L. Hao, I. Pullinen, S. Schobesberger, A. Virtanen, Isothermal evaporation of α-pinene secondary organic aerosol particles formed under low NO_x and high NO_x conditions. *Atmospheric Chemistry and Physics* **23**, 203–220 (2023).

68. G. M. Wolfe, M. R. Marvin, S. J. Roberts, K. R. Travis, J. Liao, The framework for 0-D atmospheric modeling (F0AM) v3.1. *Geoscientific Model Development* **9**, 3309–3319 (2016).

69. M. E. Jenkin, S. M. Saunders, M. J. Pilling, The tropospheric degradation of volatile organic compounds: a protocol for mechanism development. *Atmospheric Environment* **31**, 81–104 (1997).

70. S. M. Saunders, M. E. Jenkin, R. G. Derwent, M. J. Pilling, Protocol for the development of the Master Chemical Mechanism, MCM v3 (Part A): tropospheric degradation of non-aromatic volatile organic compounds. *Atmospheric Chemistry and Physics* **3**, 161–180 (2003).

71. J. F. Hunter, A. J. Carrasquillo, K. E. Daumit, J. H. Kroll, Secondary Organic Aerosol Formation from Acyclic, Monocyclic, and Polycyclic Alkanes. *Environ. Sci. Technol.* **48**, 10227–10234 (2014).

72. J. A. Thornton, C. Mohr, S. Schobesberger, E. L. D'Ambro, B. H. Lee, F. D. Lopez-Hilfiker, Evaluating Organic Aerosol Sources and Evolution with a Combined Molecular Composition and Volatility Framework Using the Filter Inlet for Gases and Aerosols (FIGAERO). *Accounts of Chemical Research* **53**, 1415–1426 (2020).

73. R. H. Schwantes, R. C. McVay, X. Zhang, M. M. Coggon, H. Lignell, R. C. Flagan, P. O. Wennberg, J. H. Seinfeld, "Science of the Environmental Chamber" in *Advances in Atmospheric Chemistry* (World Scientific, 2017)vol. 1, pp. 1–93.

74. X. Zhang, J. Ortega, Y. Huang, S. Shertz, G. S. Tyndall, J. J. Orlando, A steady-state continuous flow chamber for the study of daytime and nighttime chemistry under atmospherically relevant NO levels. *Atmos. Chem. Phys* **11**, 2537–2551 (2018).

75. D. A. Day, J. L. Fry, H. G. Kang, J. E. Krechmer, B. R. Ayres, N. I. Keehan, S. L. Thompson, W. Hu, P. Campuzano-Jost, J. C. Schroder, H. Stark, M. P. DeVault, P. J. Ziemann, K. J. Zarzana, R. J. Wild, W. P. Dubè, S. S. Brown, J. L. Jimenez, Secondary Organic Aerosol Mass Yields from NO_3 Oxidation of α-Pinene and Δ-Carene: Effect of RO_2 Radical Fate. *J. Phys. Chem. A* **126**, 7309–7330 (2022).

76. H. O. T. Pye, B. K. Place, B. N. Murphy, K. M. Seltzer, E. L. D'Ambro, C. Allen, I. R. Piletic, S. Farrell, R. H. Schwantes, M. M. Coggon, E. Saunders, L. Xu, G. Sarwar, W. T. Hutzell, K. M. Foley, G. Pouliot, J. Bash, W. R. Stockwell, Linking gas, particulate, and

toxic endpoints to air emissions in the Community Regional Atmospheric Chemistry Multiphase Mechanism (CRACMM). *Atmospheric Chemistry and Physics* **23**, 5043–5099 (2023).

77. J. Mao, F. Paulot, D. J. Jacob, R. C. Cohen, J. D. Crounse, P. O. Wennberg, C. A. Keller, R. C. Hudman, M. P. Barkley, L. W. Horowitz, Ozone and organic nitrates over the eastern United States: Sensitivity to isoprene chemistry. *Journal of Geophysical Research: Atmospheres* **118**, 11,256-11,268 (2013).

78. K. R. Travis, D. J. Jacob, J. A. Fisher, P. S. Kim, E. A. Marais, L. Zhu, K. Yu, C. C. Miller, R. M. Yantosca, M. P. Sulprizio, A. M. Thompson, P. O. Wennberg, J. D. Crounse, J. M. St Clair, R. C. Cohen, J. L. Laughner, J. E. Dibb, S. R. Hall, K. Ullmann, G. M. Wolfe, I. B. Pollack, J. Peischl, J. A. Neuman, X. Zhou, Why do models overestimate surface ozone in the Southeast United States? *Atmospheric Chemistry and Physics* **16**, 13561–13577 (2016).

79. K. H. Bates, D. J. Jacob, A new model mechanism for atmospheric oxidation of isoprene: global effects on oxidants, nitrogen oxides, organic products, and secondary organic aerosol. *Atmospheric Chemistry and Physics* **19**, 9613–9640 (2019).

80. X. Wang, D. J. Jacob, W. Downs, S. Zhai, L. Zhu, V. Shah, C. D. Holmes, T. Sherwen, B. Alexander, M. J. Evans, S. D. Eastham, J. A. Neuman, P. R. Veres, T. K. Koenig, R. Volkamer, L. G. Huey, T. J. Bannan, C. J. Percival, B. H. Lee, J. A. Thornton, Global tropospheric halogen (Cl, Br, I) chemistry and its impact on oxidants. *Atmospheric Chemistry and Physics* **21**, 13973–13996 (2021).

81. A. B. Guenther, X. Jiang, C. L. Heald, T. Sakulyanontvittaya, T. Duhl, L. K. Emmons, X. Wang, Model Development The Model of Emissions of Gases and Aerosols from Nature version 2.1 (MEGAN2. 1): an extended and updated framework for modeling biogenic emissions. *Geoscientific Model Development* **5**, 1471–1492 (2012).

82. E. E. McDuffie, S. J. Smith, P. O'Rourke, K. Tibrewal, C. Venkataraman, E. A. Marais, B. Zheng, M. Crippa, M. Brauer, R. V. Martin, A global anthropogenic emission inventory of atmospheric pollutants from sector- and fuel-specific sources (1970–2017): an application of the Community Emissions Data System (CEDS). *Earth System Science Data* **12**, 3413–3442 (2020).

83. J. Krechmer, F. Lopez-Hilfiker, A. Koss, M. Hutterli, C. Stoermer, B. Deming, J. Kimmel, C. Warneke, R. Holzinger, J. Jayne, D. Worsnop, K. Fuhrer, M. Gonin, J. De Gouw, Evaluation of a New Reagent-Ion Source and Focusing Ion-Molecule Reactor for Use in Proton-Transfer-Reaction Mass Spectrometry. *Analytical Chemistry* **90**, 12011–12018 (2018).

84. A. Zaytsev, M. Breitenlechner, A. R. Koss, C. Y. Lim, J. C. Rowe, J. H. Kroll, F. N. Keutsch, Using collision-induced dissociation to constrain sensitivity of ammonia chemical ionization mass spectrometry (NH_4^+ CIMS) to oxygenated volatile organic compounds. *Atmospheric Measurement Techniques* **12**, 1861–1870 (2019).

Acknowledgments

We thank Manjula Canagaratna of Aerodyne Research as well as Frank Keutsch and Yaowei Li of Harvard University for help with instrumentation.

Funding:
National Science Foundation Atmospheric and Geospace Science Postdoctoral Research Fellowship 2137238 (HSK)
Department of Energy grant DE-SC0022017 (MBG, CLH, JHK, NT)

Author contributions: HSK, CLH, and JHK designed the research and acquired the funding. HSK performed the model simulations and created the visualizations. HSK, NT, and MBG performed the experiments. HSK, CLH, and JHK wrote the paper with input from all authors.

Competing interests: Authors declare that they have no competing interests.

Data and materials availability: Model and experimental data shown can be found on Zenodo archive XXXXX.

Figures and Tables

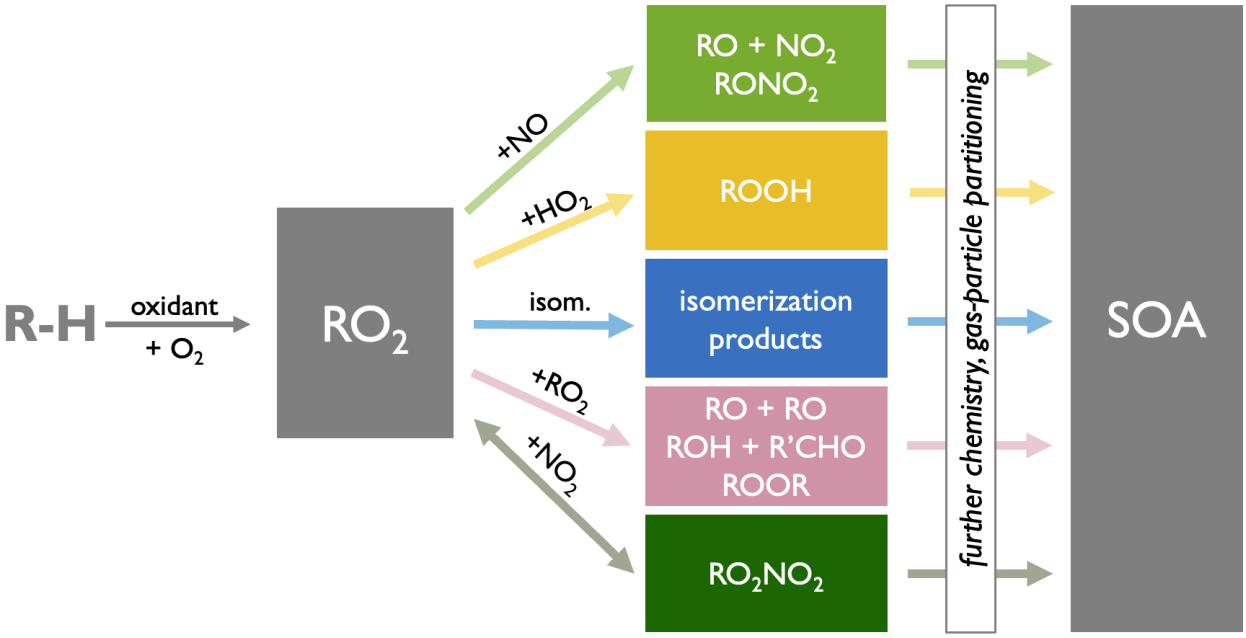

Fig 1. Schematic of atmospheric RO_2 chemistry and its role in SOA production. RO_2 are formed during VOC oxidation after initial oxidant attach and subsequent molecular oxygen addition. Atmospheric RO_2 can react bimolecularly with NO, HO_2, RO_2, and NO_2, or they can undergo unimolecular isomerization. These RO_2 reaction products can then undergo further chemistry and/or gas-particle partitioning, leading to the formation of SOA.

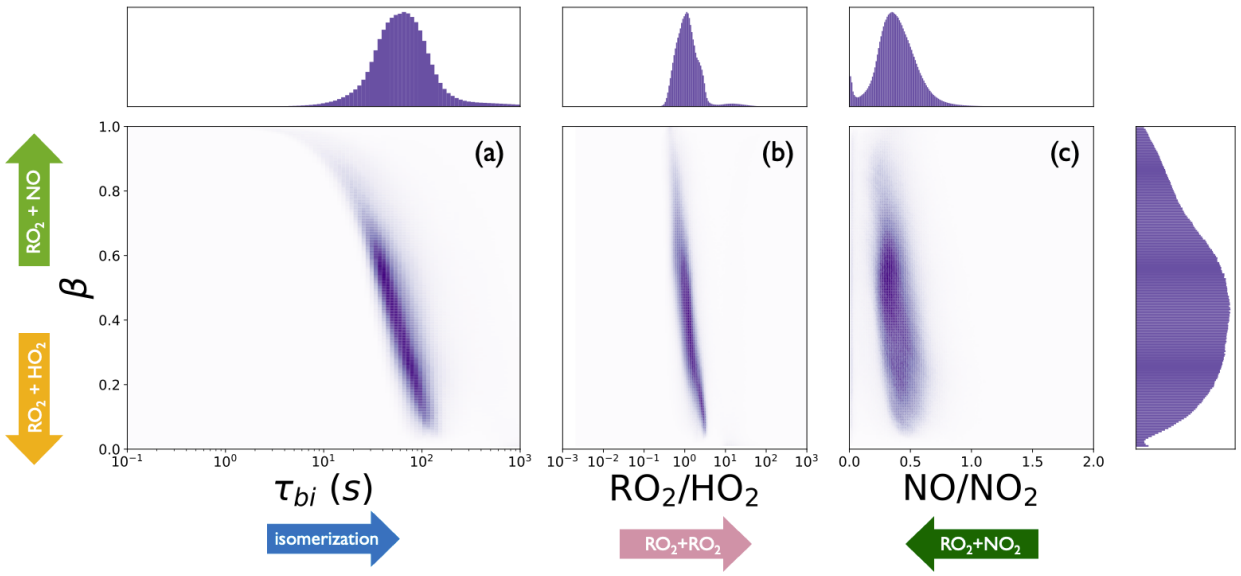

Fig. 2. Global atmospheric distribution of RO_2 fates. Shaded regions are 2D histograms of the global distribution of (**A**) β and τ_{bi}, (**B**) β and RO_2/HO_2, and (**C**) β and NO/NO_2, as predicted by GEOS-Chem in hourly output from January and July and weighted by the rate of isoprene + OH oxidation. Surrounding the 2D histograms are projections (1D histograms) of τ_{bi} (a, top), RO_2/HO_2 (b, top), NO/NO_2 (c, top) and β (c, right). β and τ_{bi} are calculated for RO_2 specific to OH-initiated oxidation of isoprene; RO_2/HO_2 is calculated with the sum of all RO_2 radicals (including CH_3O_2).

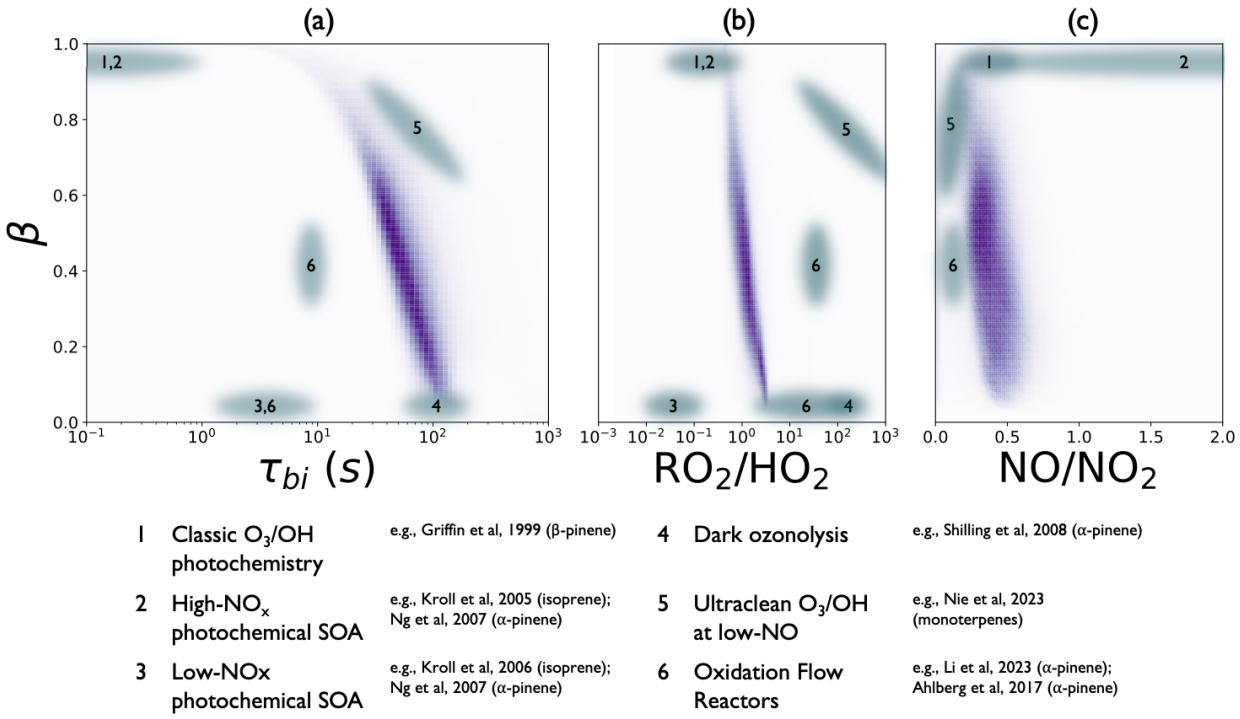

Fig. 3. Comparison of the RO_2 fate distribution achieved during previous approaches to chamber experiments with atmospheric RO_2 fate distributions. Gray ovals show the average values achieved with previous approaches to chamber experiments for (**A**) β and τ_{bi}, (**B**) β and RO_2/HO_2, and (**C**) β and NO/NO_2. In purple are the corresponding 2D histograms showing the global distribution of each parameter as predicted by GEOS-Chem (as in Figure 2). NO/NO_2 ratios are not shown for experiments with β = 0 (no NO_x). Note that RO_2+RO_2 reactions are included in the τ_{bi} calculation only for experiment type 5 and 6; in all other instances RO_2 + RO_2 reactions contribute <10% to τ_{bi} and are thus omitted for simplicity.

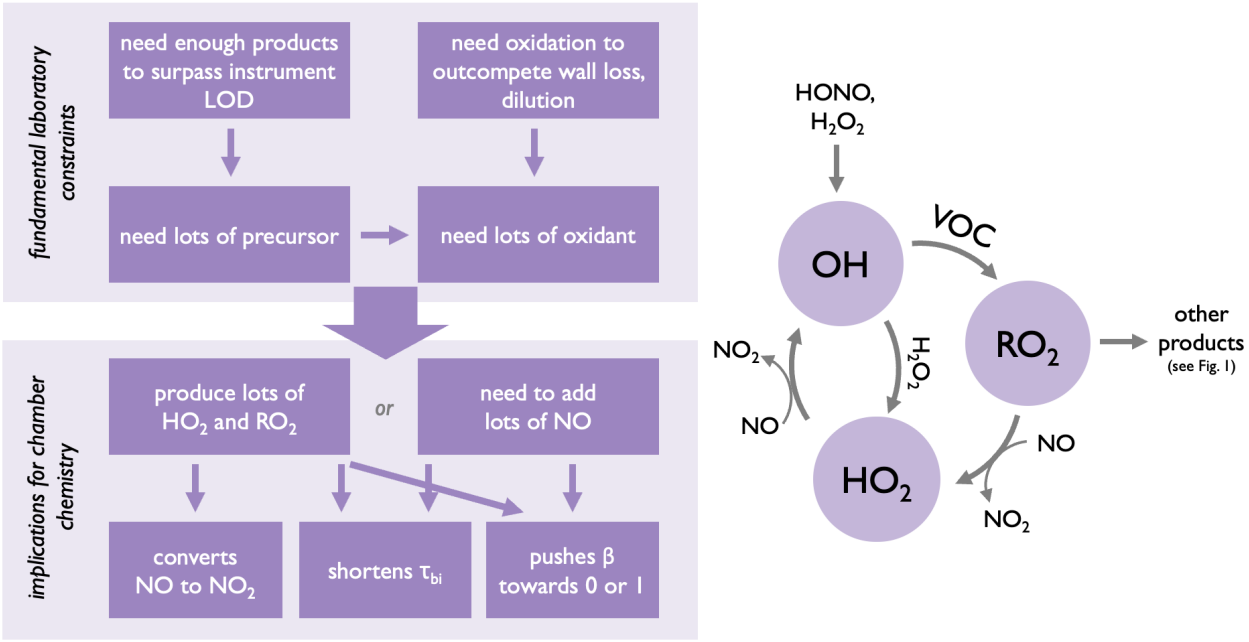

Fig. 4. Challenges of matching atmospheric conditions in chamber experiments. Left: fundamental constraints of SOA studies and implications for photochemical conditions within chambers. Right: simplified radical chemistry of the VOC oxidation chemistry that underlies such challenges.

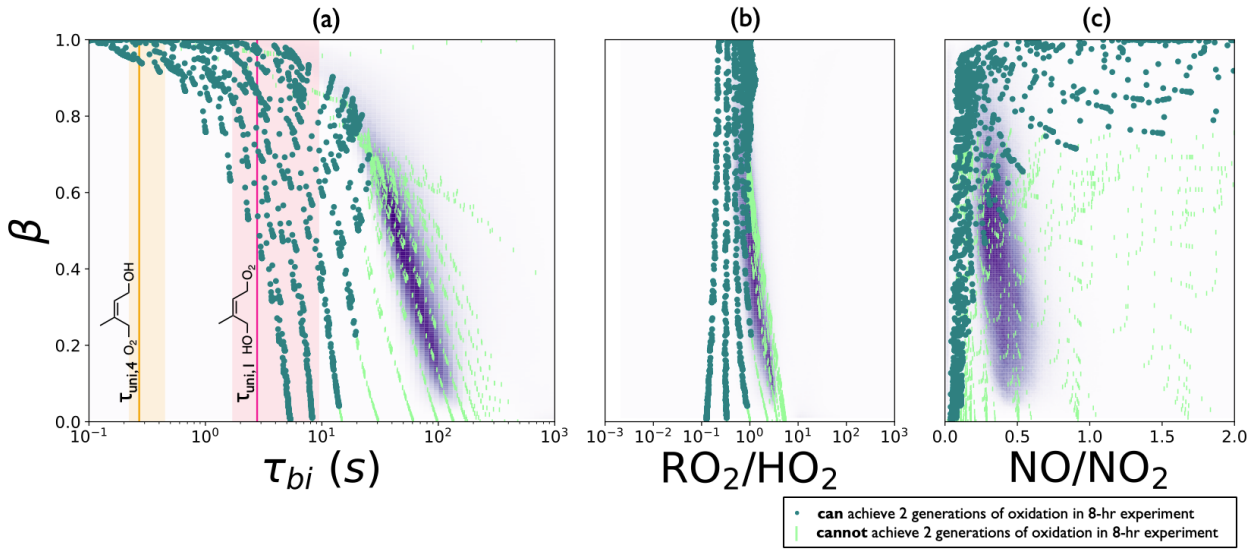

Fig. 5. Comparison of RO_2 fate distributions achievable in chambers and in the atmosphere. Points correspond to values of (**A**) β and τ_{bi}, (**B**) β and RO_2/HO_2, and (**C**) β and NO/NO_2 achievable during theoretical chamber experiments calculated with F0AM initiated with 100 ppb isoprene and different combinations of initial HONO, H_2O_2, and NO. Solid points correspond to 8-hr experiments that achieve second-generation chemistry (defined as final MVK concentration less than half of the maximum MVK concentration); lines correspond to 8-hr experiments that do not achieve sufficient second-generation chemistry. Points are overlaid on 2D histogram of the global distribution of β, τ_{bi}, RO_2/HO_2, and NO/NO_2 as predicted by GEOS-Chem (as in Figure 2). Note that β and τ_{bi} from GEOS-Chem are calculated with the corresponding atmospheric temperature and pressure whereas the chamber points are all calculated for experiments at 298 K. The unimolecular lifetimes for the two isoprene-derived RO_2 isomers that isomerize in the atmosphere are indicated in pink and orange (Teng et al, 2017). Shaded pink and orange regions indicate the range of unimolecular lifetimes that exist over the 10^{th} – 90^{th} percentile temperature range in the atmosphere during isoprene + OH oxidation.

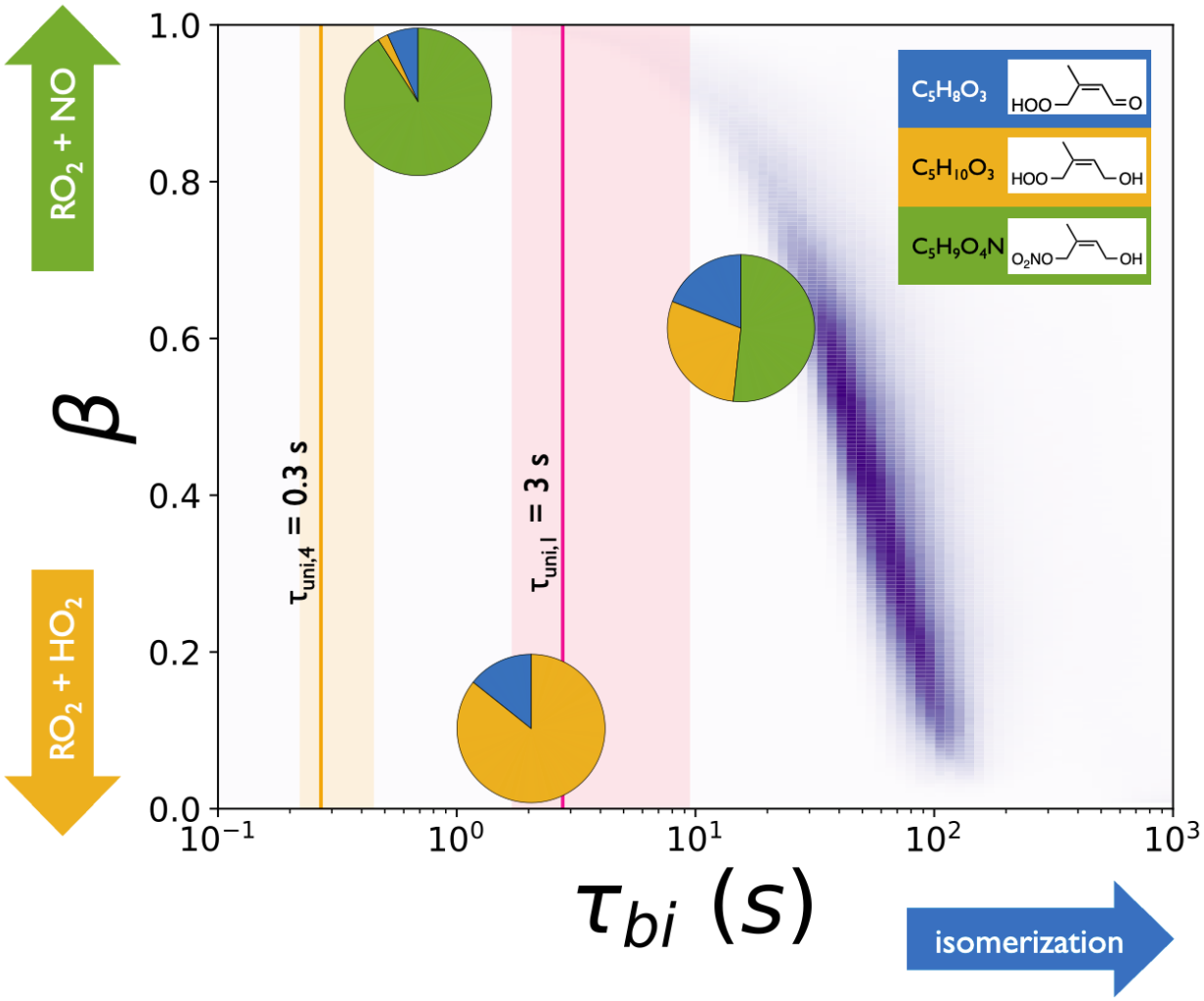

Fig. 6. Demonstration of the range of RO_2 fate distributions achievable in chamber experiments of isoprene oxidation. First generation (uncalibrated) gas-phase product yields from isoprene oxidation at a variety of β and τ_{bi} are overlaid on the atmospheric distribution of β and τ_{bi} as shown in Figure 2. The entire product distribution is not represented; rather, three masses measured by NH_4^+-CIMS representative of the three first-generation product channels are shown. Product yields are calculated as the ratio of product growth (measured by NH_4^+- CIMS) to the isoprene decay (measured by Vocus PTR) and then normalized to give the relative yields shown in the pie charts here (see Figure S9). Because the data are uncalibrated, fractions shown here should be used only to assess relative differences and are not representative of absolute product distributions. β and τ_{bi} for each experiment are calculated from modeled experiments (F0AM with MCM v3.3.1 chemistry) initialized with measured initial isoprene, HONO, NO, and NO_2 concentrations and with estimated initial H_2O_2 concentrations. Structures shown in the legend are isomers derived from the Z-*δ* 4-OH, 1-OO isoprene RO_2. The unimolecular lifetimes for the two isoprene-derived RO_2 isomers that can isomerize are indicated in pink and orange (Teng et al, 2017).